

CO₂ Capture Using Slurries of
Immobilized Deep Eutectic Solvents:
From Synthetic Gas Studies to
Flue Gas Implementation

Sahar Foorginezhad

Energy Engineering



CO₂ Capture Using Slurries of Immobilized Deep Eutectic Solvents: From Synthetic Gas Studies to Flue Gas Implementation

Sahar Foorginezhad

May 2026

Energy Engineering

Division of Energy Science

Department of Engineering Sciences and Mathematics

Luleå University of Technology

ISSN 1402-1544

ISBN 978-91-8048-997-3 (print)

ISBN 978-91-8048-998-0 (electronic)

Luleå University of Technology 2026

www.ltu.se

Abstract

The mitigation of anthropogenic CO₂ emissions requires the development of efficient, stable, and economically viable capture technologies beyond conventional amine-based systems. Deep eutectic solvents (DESs) have emerged as promising alternatives due to their tunable properties and high CO₂ affinity; however, their practical application is often limited by high viscosity and mass-transfer constraints. This thesis investigates the design, optimization, and validation of DES-based systems for CO₂ capture, with particular emphasis on combining co-solvent addition and immobilization strategies to enhance the overall performance.

In the first part, [MEACl][EDA] ([monoethanolamine hydrochloride][ethylenediamine])-based DESs with varying molar ratios were synthesized and evaluated as aqueous CO₂ absorbents. A 40 wt.% aqueous [MEACl][EDA] (1:5) system was identified as optimal, exhibiting higher CO₂ uptake (22.09 wt.% at 22 °C and 1 atm), faster absorption kinetics (1.24 mol-CO₂/(kg-sorbent·min) after 2 min at 22 °C), and comparable viscosity (4.401 mPa·s before and 13.330 mPa·s after CO₂ capture) relative to benchmark 30 wt.% aqueous monoethanolamine (MEA) (15.74 wt.% CO₂ capture capacity, viscosity of 3.318 mPa·s before and 8.413 mPa·s after CO₂ capture), along with good thermal stability and recyclability (~88% regeneration, refers to the retained CO₂ capture capacity of the sorbent after repeated sorption-desorption cycles relative to its initial capture capacity). To further improve the performance, an integration approach was developed by immobilizing 5 wt.% DES within mesoporous silica and dispersing 3 wt.% of the composite in 40 wt.%

aqueous DES to form slurries. These slurry systems demonstrated enhanced CO₂ capture capacity (up to 24.93 wt.% at 22 °C and 1 atm), improved sorption rates (1.4 mol-CO₂/(kg-sorbent·min) after 2 min at 22 °C), acceptable viscosity (7.32 and 21.82 mPa·s before and after CO₂ capture), and cyclic stability (~91% recovery).

The thesis was further extended to non-aqueous systems by immobilizing 5 wt.% DES within mesoporous silica and dispersing 3 wt.% of the composite in 20 wt.% DES in ethylene glycol as a co-solvent, resulting in improved desorption kinetics (0.38 mol-CO₂/(kg-sorbent·min) after 2 min at 110 °C), superior thermal stability, minimal solvent loss, and promising regeneration performance (~96% recovery).

Finally, this thesis investigates how gas-phase impurities and components other than CO₂, as well as the pressure, influence the performance of the developed aqueous and non-aqueous slurries. Initially, experiments with pure CO₂ and binary gas mixtures (CO₂/N₂ and CO₂/CH₄), representing major non-reactive gases commonly found in industrial streams, were tested over a wide pressure range. It shows increasing pressure enhanced CO₂ capture capacity in all systems, primarily due to increased CO₂ partial pressure; N₂ acted as an inert diluent with negligible sorption in all systems, while minor CH₄ capture capacity was observed in the non-aqueous systems. The performance of slurries was further investigated using a conditioned flue gas (pre-dried and filtered) from a biomass combustion boiler, and the presence of N₂ and O₂ as well as the trace impurities did not cause measurable competitive sorption or loss of CO₂ capture capacity.

Keywords: CO₂ capture, Flue gas, Deep eutectic solvent, Immobilization, Slurry.

Acknowledgments

This work was financially supported by the Swedish Energy Agency (2020-90040), STINT (CH2019-8287), and the Swedish Research Council (2020-03899). The research was carried out at the Division of Energy Science, Department of Engineering Sciences and Mathematics, Luleå University of Technology, Sweden.

First and foremost, I would like to express my deepest gratitude to my principal supervisor, Prof. Xiaoyan Ji, for her invaluable guidance, support, and mentorship throughout this project. Her insightful advice, encouragement, and continuous inspiration have been instrumental in shaping both my research and professional growth.

I would also like to extend my sincere thanks to my co-supervisors, Dr. Fredrik Weiland and Dr. Yifeng Chen, for their expertise, constructive feedback, and thoughtful discussions that greatly contributed to the quality and direction of this work. I am truly fortunate to have had the opportunity to learn from their knowledge and experience.

My heartfelt appreciation goes to my family for their unconditional love, understanding, and encouragement throughout my academic journey. Their patience, support, and sacrifices have been the foundation of my progress, and I am deeply grateful for their unwavering belief in me.

Finally, I would like to thank my friends for bringing joy, energy, and balance to my life during this journey. Your friendship, laughter, and support have been a constant source of strength, and I am truly grateful for your presence in my life.

Appended papers

Paper I

Foorginezhad, S., Yu, G., & Ji, X. (2022). Reviewing and screening ionic liquids and deep eutectic solvents for effective CO₂ capture. *Frontiers in Chemistry*, 10, 951951.

<https://doi.org/10.3389/fchem.2022.951951>

Sahar Foorginezhad did the literature review, screening, and writing the paper.

Paper II

Foorginezhad, S., & Ji, X. (2024). Development of monoethanolamine chloride-ethylene diamine deep eutectic solvent for efficient carbon dioxide capture. *Separation and Purification Technology*, 347, 127593.

<https://doi.org/10.1016/j.seppur.2024.127593>

Sahar Foorginezhad conducted the literature review, formulated the experimental plan, carried out the experiments, analyzed the results, and wrote the paper.

Paper III

Foorginezhad, S., & Ji, X. (2024). Developing slurry based on immobilized and aqueous [MEACl][EDA] for CO₂ capture. *Chemical Engineering Journal*, 499, 156176.

<https://doi.org/10.1016/j.ccej.2024.156176>

Sahar Foorginezhad conducted the literature review, formulated the experimental plan, carried out the experiments, analyzed the results, and wrote the paper.

Paper IV

Foorginezhad, S., & Ji, X. (2025). Developing non-aqueous slurry for CO₂ capture. *Carbon Capture Science & Technology*, 15, 100385.

<https://doi.org/10.1016/j.ccst.2025.100385>

Sahar Foorginezhad conducted the literature review, formulated the experimental plan, carried out the experiments, analyzed the results, and wrote the paper.

Paper V

Foorginezhad, S., Wikberg, E., Weiland, F., & Ji, X. (2026). Developing slurries for carbon capture: from synthetic gas Mixtures to flue gas (submitted).

Sahar Foorginezhad conducted the literature review, formulated the experimental plan, carried out the experiments, analyzed the results, and wrote the paper.

Other contributions

- I. **Foorginezhad, S.**, Chen, Y., & Ji, X. (2025). Efficient CO₂ capture using deep eutectic solvent-activated carbon slurry systems. *Colloids and Surfaces A: Physicochemical and Engineering Aspects*, 138091.
- II. **Foorginezhad, S.**, & Ji, X. (2025). Immobilized ionic liquids/deep eutectic solvents in carbon capture: current progress and future potential. *Clean Technologies and Environmental Policy*, 1-17.
- III. **Foorginezhad, S.**, Weiland, F., Chen, Y., Hussain, S., & Ji, X. (2025). Review and analysis of porous adsorbents for effective CO₂ capture. *Renewable and Sustainable Energy Reviews*, 215, 115589.
- IV. **Foorginezhad, S.**, & Ji, X. (2025). Deep eutectic solvent-based slurry for CO₂ capture: Enhanced efficiency and kinetics. *Journal of CO₂ Utilization*, 95, 103065.
- V. **Foorginezhad, S.**, & Ji, X. (2025). Enhanced CO₂ Capture Performance using Deep Eutectic Solvent-Immobilized Silica Slurry. *Results in Engineering*, 105162.
- VI. Hussain, S., Ali, A., **Foorginezhad, S.**, Chen, Y., & Ji, X. (2025). A comprehensive review on ionic liquids and ionic hybrid materials for CO₂ separation. *Separation and Purification Technology*, 360, 130997.

Contents

Abstract	i
Acknowledgements	iii
Appended papers	v
Other contributions	vii
1 Introduction	3
1.1 Background.....	3
1.2 Absorption.....	5
1.3 Ionic Liquids (ILs) and Deep Eutectic Solvents (DESs).....	8
1.4 CO ₂ capture using DES-based technologies.....	10
1.5 Objectives.....	12
2 Materials and methods	18
2.1 Materials.....	18
2.2 Preparation of materials.....	19
2.2.1 [MEACl][EDA] DES.....	19
2.2.2. Aqueous and non-aqueous [MEACl][EDA].....	19
2.2.3. Immobilization of [MEACl][EDA] on solid.....	20
2.2.4. Slurry formulation.....	20
2.3 Characterization of materials.....	21
2.4 CO ₂ sorption/desorption measurements.....	22
2.4.1 CO ₂ sorption.....	22
2.4.2 CO ₂ desorption.....	27
2.5 Kinetics.....	28
3 Results and discussion	32

3.1 DES and substrate selection	32
3.1.1 Identification of DESs and further studies	32
3.1.2 Substrate selection	36
3.2 Identification of the optimal aqueous DES	37
3.2.1 CO ₂ sorption performance	37
3.2.2 Viscosity	39
3.2.3 FTIR analysis	42
3.2.4 Effect of temperature on CO ₂ capture capacity	43
3.2.5 Absorption-desorption cyclic performance.....	44
3.2.6 Kinetics	45
3.3 Integration of immobilization and co-solvent addition.....	46
3.3.1 Structural characteristics of immobilized DES	47
3.3.2 Aqueous slurry	47
3.3.2.1. CO ₂ sorption measurements	47
3.3.2.2. Effect of temperature	50
3.3.2.3. Viscosity	51
3.3.2.4. Stability	52
3.3.2.5. FTIR analysis	53
3.3.2.6. Cyclic performance	54
3.3.2.7. Kinetics	55
3.3.3 Non-aqueous slurry	56
3.3.3.1. CO ₂ sorption measurements	56
3.3.3.2. Viscosity	59
3.3.3.3. Stability	60
3.3.3.4. FTIR analysis	60
3.3.3.5. Cyclic performance	61
3.3.3.6. Kinetics	62
3.4 Further studies	63
3.4.1 CO ₂ sorption using pure CO ₂ and synthetic gas mixtures	63
3.4.2 CO ₂ sorption using conditioned flue gas from CHP boiler	66
4 Conclusions.....	72
5 Future work	76
6 References	80

Chapter 1

1 Introduction

1.1 Background

The rapid rise in greenhouse gas (GHG) concentrations in the atmosphere has become one of the most pressing challenges of our time, driving global climate change and environmental issues [1]. As the world population grows and economies expand, the demand for energy continues to escalate, creating a complex challenge of balancing economic development with environmental sustainability [2]. Despite ongoing efforts to diversify energy sources, fossil fuels, such as coal, oil, and natural gas, remain the dominant contributors to the global energy supply [3, 4]. However, their extensive use releases vast amounts of carbon dioxide (CO₂), the primary anthropogenic GHG responsible for global warming. Studies have shown a near-linear relationship between cumulative CO₂ emissions and the increase in global average temperature over long-time scales, emphasizing the urgent need to mitigate CO₂ emissions.

Achieving international climate targets, such as limiting global temperature rise to 1.5 or 2 °C, requires not only expanding clean energy sources but also developing effective strategies to manage and mitigate emissions from existing fossil fuel use [5-7]. In this context, carbon capture, utilization, and storage (CCUS) technologies are widely considered as key mitigation strategies for achieving net-zero emission targets. CCUS encompasses the capture of CO₂ from large stationary sources, including power plants and industrial facilities, followed by its utilization and/or its long-term geological storage [8]. The captured CO₂ can be converted into valuable products such as fuels, chemicals, or building materials, thereby reducing dependence on fossil resources [9]. Alternatively, it can be securely stored in geological formations or

mineralized to achieve long-term carbon removal and prevent its release into the atmosphere [10, 11].

CO₂ capture step represents a critical stage within the CCUS framework and can be achieved through three main approaches: pre-combustion, post-combustion, and oxy-fuel combustion methods [12]. In post-combustion capture, CO₂ is separated from flue gases produced during the combustion of fossil fuels in power plants or industrial facilities, making it one of the most applicable and flexible techniques for existing infrastructures [13]. Pre-combustion capture, on the other hand, involves the partial oxidation or gasification of fuels to produce synthesis gas (syngas), which is subsequently treated to remove CO₂ and yield a hydrogen-rich stream suitable for clean energy applications [14]. In oxy-fuel combustion, fuel is burned in a mixture of pure oxygen and recycled flue gas, producing an exhaust composed mainly of CO₂ and water vapor, thereby simplifying the separation process [12, 15]. Among these, post-combustion CO₂ capture is considered the most technologically mature and readily deployable option due to its compatibility with current fossil fuel-based energy systems and industries such as cement, steel, and iron production [16].

In terms of post-combustion CO₂ capture, several techniques are employed for this purpose, including absorption, adsorption, membrane separation, and cryogenic separation. The selection of an appropriate method depends on various factors, such as the composition and temperature of the flue gas, CO₂ concentration, flow rate, and regulatory discharge requirements [17]. Among these, absorption has emerged as the most mature and commercially feasible technology, offering high

efficiency and continuous operation, which makes it an attractive option for large-scale deployment and further technological advancement [18].

1.2 Absorption

Absorption is currently regarded as one of the most established and effective techniques for CO₂ capture due to its technological maturity, operational flexibility, and suitability for both large-scale industrial facilities and power plants [16, 19]. In this process, CO₂ is selectively separated from a gas mixture by transferring it into a liquid phase using a solvent. Based on the interaction mechanism between the solvent and CO₂, the process is broadly categorized into physical and chemical absorption [20].

In physical absorption, CO₂ dissolves physically into the solvent according to Henry's law, where solubility increases with pressure and decreases with temperature. The absorbed CO₂ is typically released by reducing the pressure, although temperature increase or a combination of pressure and temperature changes may also be applied for regeneration [19, 21]. Physical solvents, such as methanol (Rectisol), propylene carbonate (PC), and dimethyl ethers of polyethylene glycol (DEPG, known as Selexol), are typically employed in systems with high CO₂ partial pressures, including pre-combustion processes, syngas treatment, and natural gas purification. In these systems, CO₂ is absorbed through physical dissolution rather than chemical reaction, and therefore solvent regeneration generally requires lower energy. However, their CO₂ capture capacity significantly decreases at low partial pressures, limiting their applicability for post-combustion scenarios [21, 22].

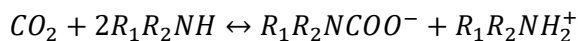
In contrast, chemical absorption utilizes reactive solvents that form chemical bonds with CO₂ molecules, enabling efficient separation even

at low partial pressures typical of flue gases (3–20 vol% CO₂) [19, 21]. This process generally employs aqueous amine solutions, such as monoethanolamine (MEA), diethanolamine (DEA), and methyldiethanolamine (MDEA), which have been widely used for decades [23–25]. MEA, in particular, remains a benchmark solvent because of its high reactivity with CO₂, ease of handling, and relatively low cost. The basic process involves CO₂ absorption in an absorber column, where flue gas is passed counter-currently to the liquid solvent at moderate temperatures (40–60 °C) [25]. The CO₂-rich solvent is then directed to a stripper column, where heating (typically 100–120 °C) regenerates the solvent and releases CO₂, which can be compressed for utilization or storage within CCUS systems [19, 21]. Here, the type of amine plays a crucial role in determining performance metrics, including CO₂ capture capacity, sorption kinetics, regeneration energy requirements, and operational stability [26]. In addition, the reaction mechanism between CO₂ and amines is highly dependent on the amine structure. Primary and secondary amines typically react with CO₂ to form carbamate species, whereas tertiary amines predominantly produce bicarbonate in aqueous environments [27]. The representative reactions are outlined below:

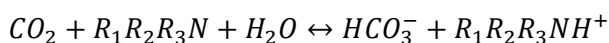
Primary amines:



Secondary amines:



Tertiary amines:



The distinct reaction mechanisms largely explain the variation in performance among different amines. Primary and secondary amines react with CO₂ to produce relatively stable carbamate species, leading to fast sorption rates and comparatively high capture capacities; however, this process requires two amine molecules per CO₂ molecule. In contrast, tertiary amines promote the formation of bicarbonate in aqueous media via a 1:1 stoichiometry, which allows higher molar loading and facilitates CO₂ desorption, thereby reducing regeneration energy requirements. This behavior is attributed to the presence of an active hydrogen atom in primary and secondary amines that enables carbamate formation, whereas tertiary amines lack such a reactive site [28, 29].

Despite its widespread industrial adoption, chemical absorption faces several challenges. The process is energy-intensive, with the regeneration step accounting for a major portion of the overall energy cost. Moreover, amine-based solvents are prone to thermal and oxidative degradation, corrosion, and the formation of unwanted by-products during prolonged operation [19, 30, 31]. These drawbacks have driven intensive research into alternative solvent systems aimed at improving absorption capacity, reaction kinetics, and solvent recyclability while minimizing environmental and economic impacts.

Recent developments include the design of blended amine systems, for instance, combinations of MEA with sterically hindered or tertiary amines such as piperazine (PZ) or MDEA, to enhance absorption performance and lower energy requirements for solvent regeneration [32-34]. Additionally, phase-change solvents have gained attention for their ability to form biphasic systems during CO₂ capture, reducing the volume of solvent that needs to be regenerated. Likewise, deep eutectic solvents (DESs) and ionic liquid (IL)-based systems are being explored as next-

generation alternatives because of their tunable properties, negligible volatility, and potential for lower regeneration energy [19].

1.3 Ionic Liquids (ILs) and Deep Eutectic Solvents (DESs)

ILs are salts composed entirely of ions that remain liquid at or near ambient temperature, typically with melting points below 100 °C [35]. They generally consist of an organic cation combined with an organic or inorganic anion [36]. Because of their ionic structure, ILs exhibit a series of remarkable physicochemical properties, including extremely low vapor pressure, high thermal stability, non-flammability, and strong polarity [25]. These features have led to their application in a wide range of disciplines such as catalysis, electrochemistry, materials science, and separation processes [37, 38]. In particular, their negligible volatility and thermal robustness make them attractive alternatives to conventional volatile organic solvents in gas absorption and separation.

In CO₂ capture applications, ILs can act as either physical or chemical absorbents depending on their composition and the type of interaction between the ionic species and CO₂ molecules [39]. Experimental studies have shown that the solubility of CO₂ in ILs depends strongly on the anion, while the cation has a smaller effect. In terms of physical ILs, those containing bis(trifluoromethylsulfonyl)imide ([Tf₂N]⁻), tetrafluoroborate ([BF₄]⁻), or hexafluorophosphate ([PF₆]⁻) anions demonstrate higher CO₂ solubility compared with those containing acetate or chloride [40]. Regarding chemical ILs, Bates et al. [41] introduced amine-functionalized ILs, commonly termed task-specific ionic liquids (TSILs), designed to promote chemical binding with CO₂. These functionalized ILs exhibit significantly higher uptakes and more selective absorption behavior than

non-reactive systems, while still maintaining the intrinsic non-volatility and tunability of the IL family.

Despite these advantages, ILs are constrained by practical limitations, particularly their high viscosity and relatively high cost. The strong interactions between cations and anions contribute to high viscosity and reduce mass-transfer efficiency during gas absorption [25].

Deep eutectic solvents (DESs) have recently emerged as promising analogues or alternatives to ILs. Introduced by Abbott et al. [42, 43], DESs are typically composed of at least two components: a hydrogen-bond acceptor (HBA) and a hydrogen-bond donor (HBD), that self-associate to form a eutectic mixture with a melting point far lower than those of the individual constituents [44]. The most common HBAs are quaternary ammonium salts such as choline chloride, while the HBDs can include urea, glycerol, ethylene glycol, or carboxylic acids [45]. This strong hydrogen-bond network leads to the depression of the melting point, often rendering a liquid mixture at room temperature. DESs share many favorable properties with ILs, including low volatility, non-flammability, and thermal stability, but they offer additional advantages such as ease of preparation, low cost, and the use of environmentally benign and biodegradable precursors [46, 47].

In the context of CO₂ capture, DESs can also function via physical or chemical absorption mechanisms. Conventional, or non-functionalized, DESs primarily absorb CO₂ physically through physical dissolution within the hydrogen-bonded network. For example, Li et al. [48] examined CO₂ solubility in choline-chloride-based DESs at various molar ratios and conditions, showing that CO₂ uptake generally increases with pressure and decreases with temperature, similar to traditional physical solvents.

However, due to limited CO₂ capture capacity arising from purely physical interactions, researchers have developed functionalized DESs, incorporating active sites such as amine or superbase groups to chemically bind CO₂ [49, 50]. These systems, sometimes referred to as task-specific DESs, exhibit higher CO₂ capture capacities due to reversible chemical interactions between CO₂ and functional moieties within the solvent. Despite mitigating several limitations of ILs, DESs still have relatively high viscosity, which restricts gas diffusion. Continued research and development are therefore essential to improve their performance and scalability in CO₂ capture systems.

1.4 CO₂ capture using DES-based technologies

The high viscosity of DESs, similar to that observed in many ILs, remains a critical limitation for efficient CO₂ capture. To mitigate this issue, two principal strategies have been developed. The first involves the incorporation of a low-viscosity co-solvent, typically water or short-chain alcohols, to dilute the DES matrix. This approach effectively reduces viscosity and enhances gas diffusivity; however, excessive dilution can compromise CO₂ capture capacity of the system [51, 52]. Thus, an optimal balance between fluidity and absorption performance must be carefully maintained. A second approach is based on the immobilization of DESs in porous solid supports to form composite materials. In this configuration, a limited amount of DES is dispersed over a high-surface-area substrate, which shortens diffusion paths and facilitates faster gas-liquid interactions [53-56]. A wide range of porous materials such as silica, alumina, ZIFs (zeolitic imidazolate frameworks), MOFs (metal-organic frameworks), zeolites, polymeric particles, and carbon-based structures have been used for this purpose [57-60]. However, certain challenges

persist. The immobilized layer can hinder CO₂ diffusion if the DES film becomes excessively thick, leading to reduced overall capture capacity. Furthermore, practical implementation in continuous or industrial operations is more challenging compared to liquids and often constrained by the stability of the coated layer, potential leaching of the DES phase, and regeneration complexity [61]. Both two existing strategies have been largely studied independently, and in particular, water has been widely investigated as one co-solvent. However, their potential combined effect has not yet been systematically examined.

In principle, mixing aqueous or co-solvent added DESs with immobilized DESs can form a slurry system that is suitable for continuous operation and takes advantage of the benefits of both methods. Such a configuration may offer synergistic advantages by simultaneously reducing mass transfer limitations through viscosity control and enhancing interfacial contact via immobilization. Indeed, previous studies indicate that CO₂ capture performance can be improved by suspending solid adsorbents in amine-based solvents, including enhanced CO₂ uptake, improved desorption rates, reduced regeneration energy requirements [62] as well as elevated sorption rates [63, 64]. On the other hand, it is also found that increasing the fraction of immobilized DES in slurry systems also leads to higher viscosity, which can hinder fluid circulation and reduce gas-liquid mass transfer efficiency [65-71].

In summary, to the best of our knowledge, no previous investigation has evaluated the integrated approach of combining co-solvent addition with immobilization to determine its effectiveness for CO₂ capture. In this configuration, fine solid particles are suspended within a liquid phase, forming a slurry, and the content of the slurry is one of the main factors that needs to be considered.

1.5 Objectives

The primary objective of this thesis is to investigate the potential synergistic effects of combining co-solvent addition and immobilization in the form of a slurry for CO₂ capture. This thesis aims to evaluate whether integrating viscosity reduction through co-solvent addition with enhanced interfacial contact provided by immobilization can improve overall CO₂ capture performance. Particular attention is given to assessing changes in CO₂ capture and sorption rate, as well as the feasibility of operating such system in a continuous mode. Further development in this area is crucial to optimize the system stability and assess the performance under realistic operating conditions.

Based on these objectives, the overarching research questions of this thesis are listed below:

1. Do immobilized DES slurries exhibit improved CO₂ sorption, desorption, and cyclic stability compared to diluted DES and commercial MEA?
2. How does the presence of N₂ and O₂ influence CO₂ uptake in the developed slurries?
3. What is the CO₂ capture performance of the developed slurries under elevated pressures relevant to industrial applications and when exposed to flue gas?

To answer these research questions, the thesis is structured around the following specific objectives:

- a) Comprehensive literature review to select DES and substrate

The first stage of the work involved a literature review to identify the most promising materials and design strategies for CO₂ capture. This

review covered three major themes: (i) ILs and DESs used for CO₂ capture to understand the current state of research and identify the most effective ones (one review paper was published and appended to this thesis); (ii) various types of porous solids employed for CO₂ capture to determine a suitable substrate for further study; and (iii) immobilized IL and DES systems, emphasizing the CO₂ capture performance. Insights from these reviews provided a clear direction for the subsequent experimental design and material selection in this research. One DES and substrate were selected in this step.

b) Formulation and optimization of aqueous DESs

After selection of the type of DES, various molar ratios of HBA to HBD were prepared to further investigate their CO₂ uptake and viscosity. This step aimed to identify the optimal composition by evaluating the influence of HBA:HBD ratios on absorption performance and rheological behavior. Subsequently, the selected DES formulations were diluted with water as a co-solvent to improve mass transfer and sorption kinetics. The water content and DES composition were varied to enhance CO₂ capture capacity while maintaining suitable viscosity. The primary focus of this stage was the optimization of CO₂ capture performance and viscosity. The findings from this work led to the publication of one research article and appended to this thesis.

c) Formulation and optimization of slurry systems

Following the optimization of the aqueous DES formulations, a range of immobilized DESs were prepared and subsequently combined with the optimized aqueous DES to develop slurries. This approach was designed to integrate the high surface area advantages of solid-supported DES with the enhanced mass transfer and compositional tunability of aqueous DES

systems. The primary objective of this stage was to evaluate the feasibility of the slurry concept for CO₂ capture applications. Key performance indicators, including CO₂ capture capacity, sorption kinetics, viscosity, recyclability, and overall process stability, were investigated to assess the technical viability of the integrated sorbent system. The outcomes of this work resulted in the publication of one research article and appended to this thesis.

Due to the high energy demand associated with water evaporation during regeneration, stemming from its high specific heat capacity and enthalpy of vaporization, which increase both sensible and latent heat requirements [72-74], ethylene glycol (EG) was selected as an alternative co-solvent due to its favorable physicochemical properties, namely, a lower specific heat capacity (2.43 J/g·°C at 25 °C), a high boiling point (197.3 °C), and low vapor pressure (0.032 bar at 25 °C) [75]. Non-aqueous EG-based slurry systems were studied. The objective of this stage was to enhance the desorption performance while minimizing solvent loss and reducing desorption time. The findings from this study resulted in the publication of one research article and appended to this thesis.

- d) Further studies using pure and synthetic gas mixtures at high pressures and flue gas at atmospheric pressure

Following laboratory-based optimization, the CO₂ capture of the developed slurries was evaluated using pure and synthetic gas mixtures (CO₂/N₂ and CO₂/CH₄, representing major non-reactive gases commonly found in industrial streams) under pressurized conditions (up to 1.5 MPa) to simulate industrial operating environments. The influence of gas impurities and mixed-gas compositions was analyzed. Finally, the slurries' performance was studied using a conditioned flue gas collected

from the combined heat and power (CHP) boiler at Smurfit WestRock in Piteå, Sweden, where the exhaust stream is generated from biomass combustion then pre-dried and filtered (particulate removal). One research paper is submitted and appended to this thesis.

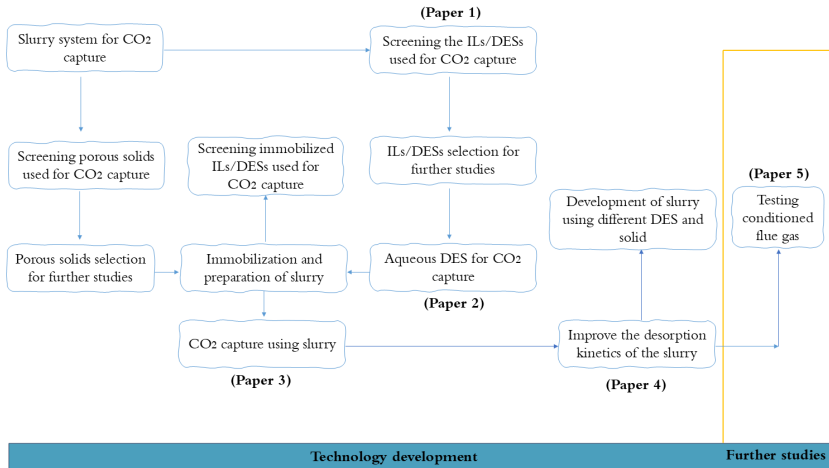


Fig. 1-1. The overview of how the appended papers relate to the specific objectives.

Chapter 2

2 Materials and methods

The following sections present a description of the chemicals, materials, and experimental methodologies employed throughout this thesis. These include the preparation of pure DESs, the immobilization of DESs onto solid supports, and the preparation of both aqueous and non-aqueous DES systems, as well as DES-based slurries. Furthermore, experimental procedures used for material characterization and for evaluating CO₂ capture performance under varying pressures and temperatures are described.

2.1 Materials

Hydrochloric acid (HCl, 37%) was obtained from VWR Chemicals. Ethylenediamine (EDA, synthesis grade) and ethanol (EtOH, analytical grade, $\geq 99.5\%$ purity) were purchased from Merck, while monoethanolamine (MEA, $\geq 98\%$) and ethylene glycol ((CH₂OH)₂, 99.8%) were bought from Sigma-Aldrich. Mesoporous silica (SBA-15, 99.9% purity, surface area 200–500 m²/g, pore diameter 12 nm) was also acquired from Merck. High-purity gases, including CO₂ and N₂ (ANAEROB, 99.99% purity), were provided by Linde Gas. Ultrapure water was produced using a Milli-Q[®] purification system. CO₂/N₂ (25/75 vol/vol%) and CO₂/CH₄ (40/60 vol/vol%) gas mixtures were purchased from AGA AB (Linde group). Flue gas was obtained from a CHP biomass boiler at Smurfit WestRock, Piteå, Sweden, and then pre-dried and filtered (particulate removal) before being fed into a 10-L gas-sampling bag.

2.2 Preparation of materials

2.2.1 [MEACl][EDA] DES

The synthesis of monoethanolammonium chloride (MEACl) was carried out in accordance with the procedure reported by Trivedi et al. [76]. Briefly, MEA was protonated by the gradual addition of an equimolar amount of HCl under continuous stirring in an ice bath maintained at 0 °C. Then, the resulting solution was heated at 60 °C for 3 h. The excess water was subsequently removed using a rotary evaporator under reduced pressure, followed by additional drying under ultra-high vacuum at 60 °C for 6 h to eliminate any residual moisture.

The synthesized MEACl, serving as the HBA, was then mixed with EDA, acting as the HBD, in varying molar ratios ranging from (1:1) to (1:10). The mixtures were stirred for 30 min to ensure homogeneity, after which vacuum drying was applied to remove any remaining moisture.

2.2.2. Aqueous and non-aqueous [MEACl][EDA]

Aqueous DES samples were prepared by mixing different concentrations of pure [MEACl][EDA], with varying HBA:HBD molar ratios, with deionized water, as co-solvent, to obtain mixtures containing 40-70 wt.% DES [51].

Non-aqueous DES systems were prepared using EG as a co-solvent. Different quantities of [MEACl][EDA] were mixed with EG to obtain homogeneous mixtures [77].

2.2.3. Immobilization of [MEACl][EDA] on solid

Commercial mesoporous silica particles were utilized directly as support for the immobilization of DES without any prior surface modification. To remove residual moisture, the silica particles were first dried in a vacuum oven at 120 °C for 24 h. The immobilization of [MEACl][EDA] onto the silica was carried out using a two-step impregnation–evaporation procedure [78, 79]. In this method, different amounts of [MEACl][EDA] were mixed with ethanol, and after 30 min of mixing, a defined quantity of the pre-dried silica (typically 0.1 g) was added to the solution to achieve targeted DES loadings of 3, 5, 10, and 15 wt.%. The suspension was stirred while the solvent was evaporated at 45 °C. The resulting powder was subsequently dried in a vacuum oven at 70 °C for 24 h. The final [MEACl][EDA]-functionalized silica samples were obtained with varying DES loadings and were labeled as x -[MEACl][EDA]@silica, where x corresponds to the DES loading level (0, 3, 5, 10, and 15 wt. %).

2.2.4. Slurry formulation

Aqueous slurries were prepared using a blending approach [80]. Initially, an aqueous solution of [MEACl][EDA] was prepared. Subsequently, different amounts of x -[MEACl][EDA]@silica sorbents, corresponding to loadings from 0.1 to 7 wt. %, were added to the DES solution. The mixture was then subjected to stirring for 30 min using both a mechanical stirrer and an ultrasonic bath to ensure uniform dispersion of the solid particles.

For the preparation of non-aqueous slurries, varying amounts of [MEACl][EDA] were mixed with EG. Following the procedure adopted for the preparation of aqueous slurry, 3 wt.% of 5-[MEACl][EDA]@silica

was incorporated into the DES-EG mixture. The resulting suspension was stirred for 30 min to achieve a uniform dispersion [77].

2.3 Characterization of materials

The melting points of [MEACl][EDA] with various molar ratios were determined using a Differential Scanning Calorimeter (DSC 821e, METTLER TOLEDO Co.). Measurements were conducted over a temperature range of -80 to 80 °C at a heating rate of 2 °C/min under a nitrogen atmosphere.

The chemical composition and bonding characteristics of pure [MEACl][EDA], aqueous and non-aqueous [MEACl][EDA], immobilized [MEACl][EDA], and the prepared slurries were analyzed using Fourier Transform Infrared Spectroscopy (FTIR), both before and after CO₂ capture. A VERTEX 70v spectrometer (BRUKER Co.) was employed to perform these measurements.

The viscosities (η) of pure and aqueous MEA, EDA, [MEACl][EDA], as well as non-aqueous [MEACl][EDA], both before and after CO₂ capture, were measured using a Microviscometer (Anton Paar, Lovis 2000 ME). The temperature was controlled with an uncertainty of 0.01 °C, and the instrument's accuracy was 0.50%. Each measurement was repeated at least three times, and its average value was recorded with the standard deviation found to be generally within ± 0.0054 mPa·s.

The viscosities (η) of the aqueous and non-aqueous slurries, both before and after CO₂ capture, were determined using an Anton Paar rheometer (MCR 92) interfaced with RheoCompassTM software. Each measurement was repeated at least three times, and its mean value was

reported. The standard deviation of the measurements was found to be ± 0.2 mPa·s.

Nitrogen adsorption-desorption isotherms of both pure and [MEACl][EDA]-immobilized silica samples were measured at -196 °C using a BELSORP MAX X analyzer. Prior to analysis, the samples were degassed at 85 °C under a pressure of 1 Pa for 4 h. The specific surface area was calculated using the Brunauer–Emmett–Teller (BET) method, while the total pore volume was determined from the amount of nitrogen adsorbed at a relative pressure of $P/P_0 = 1$. Pore size distributions were obtained from the desorption branch of the isotherms using the Barrett–Joyner–Halenda (BJH) method.

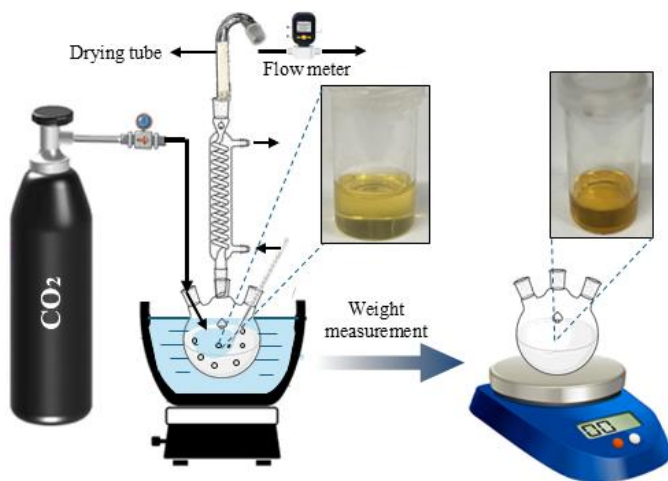
2.4 CO₂ sorption/desorption measurements

2.4.1 CO₂ sorption

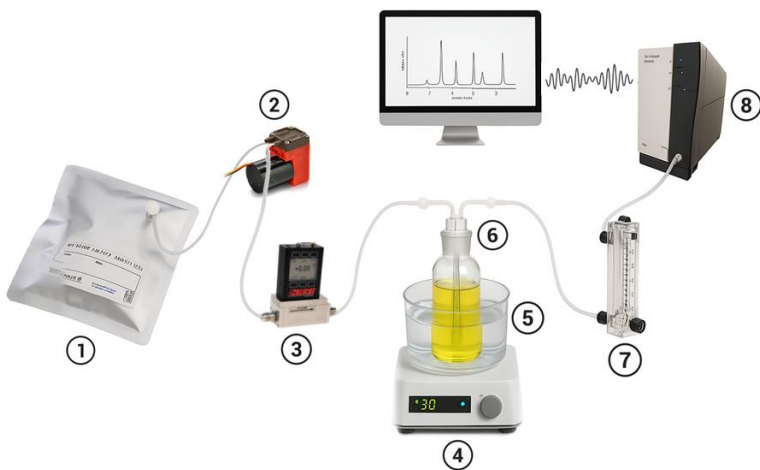
a) Sorption at atmospheric pressure: CO₂ capture experiments at atmospheric pressure were carried out by bubbling CO₂ gas into vials containing the desired samples. The CO₂ flow rate was maintained at 100 mL/min using a 100 SCCM flow controller with an accuracy of $\pm 0.6\%$ of the reading. The setup was fitted with a drying tube filled with silica gel and a condenser to minimize water loss through evaporation. The CO₂ uptake was determined gravimetrically by periodically weighing the system to record the incremental mass corresponding to the captured CO₂ (Fig. 2-1(a)). Each CO₂ sorption experiment was repeated three times, and the average values were reported. The standard deviation of the measurements was within ± 0.03 wt.%.

The CO₂ capture performance of both aqueous and non-aqueous slurry systems was investigated using conditioned flue gas obtained from

the combined heat and power (CHP) unit at Smurfit WestRock (Piteå, Sweden) after pre-drying and particulate removal through filtration. The collected gas was stored in a 10 L sampling bag (①) and fed into the experimental setup. A pump (②) was used to deliver the gas continuously, while the flow rate was controlled at 100 mL/min using a mass flow controller (③). The gas stream was then introduced into a sorption bottle (⑥), which was placed in a thermostated water bath (⑤) maintained at 25 °C and atmospheric pressure (1 bar) using a magnetic stirrer-hotplate (④). The outlet stream passed through a secondary flow meter (⑦) prior to composition analysis. Gas composition was measured using an Agilent 490 Micro Gas Chromatograph (⑧) at 20 s intervals. The CO₂ uptake was calculated from the difference between inlet and outlet CO₂ concentrations over time under continuous flow conditions. The outlet flow rate fluctuated within ± 0.05 NL/h, while the inlet CO₂ concentration varied between 11.8 and 12.7% depending on the gas source. The feed gas primarily consisted of N₂ (73.2–78.8%), CO₂ (11.8–12.7%), and O₂ (10.4–14.4%), with trace amounts of CO and CH₄ (<0.02%). Gas compositions at both the inlet and outlet were analyzed using a micro-GC, with the inlet composition measured prior to each experiment and used for subsequent mass balance calculations. The overall measurement uncertainty was estimated at $\pm 2.8\%$ (Fig. 2-1(b)).



(a)



(b)

Fig. 2-1. The lab-scale setup for CO_2 capture using (a) pure CO_2 (adapted with permission from [81]) and (b) flue gas (1. Gas bag, 2. Pump, 3. Gas flow controller, 4. Heater/stirrer, 5. Water bath, 6. Sorption bottle, 7. Gas flow meter, and 8. Micro-GC gas analyzer).

b) Sorption at elevated pressures: CO₂ capture at pressures higher than the atmospheric condition was investigated using a vapor-liquid equilibrium (VLE) apparatus, as illustrated in Fig. 2-2. Experiments were conducted at pressures up to 1.5 MPa using pure CO₂ and synthetic gas mixtures. The setup consisted of a gas reservoir, an equilibrium cell equipped with a magnetic stirrer, a thermostatic water bath for precise temperature control, and two high-accuracy pressure sensors. In each experiment, specified amount of sorbent was placed in the equilibrium cell, which was subsequently evacuated with a vacuum pump to remove residual gases; this brief evacuation step was assumed to have negligible effects on the solvent properties. Gas was then introduced by opening the valve connecting the gas reservoir to the equilibrium cell.

Each experiment was conducted in triplicate to ensure reproducibility. Pressures in both the gas reservoir and equilibrium cell were continuously monitored and used to calculate the amount of gas component (*i*) captured by the known mass of sorbents. For pure CO₂, solubility was determined from the pressure differences between the gas reservoir and equilibrium cell before and after equilibrium, as expressed in Eqs. (2-1) and (2-2):

$$n_i = \frac{p^{0,GR}V_{GR}}{Z_1RT} - \frac{p^{eq,GR}V_{GR}}{Z_2RT} - \frac{(p^{eq,EC} - p^s)(V_{EC} - V_s - V_r)}{Z_3RT} \quad (2-1)$$

$$x_i = \frac{n_i}{n_{gas} + n_{DES} + n_{co-solvent} + n_{SiO_2}} \quad (2-2)$$

where $p^{0,GR}$ denotes the initial pressure in the gas reservoir, $p^{eq,GR}$ and $p^{eq,EC}$ correspond to the equilibrium pressures in the gas reservoir and the equilibrium cell, respectively. p^s represents the saturated vapor pressure of the sorbent at temperature T , R is the universal gas constant, and Z_1 , Z_2 , and Z_3 are the compressibility factors of gas i at pressures $p^{0,GR}$, $p^{eq,GR}$, and

$(p^{eq,EC} - p^s)$, respectively. V_{GR} , V_{EC} , and V_r refer to the volumes of the gas reservoir, equilibrium cell, and magnetic rotor, while V_s denotes the sorbent volume. The mole fraction of component i in the liquid phase is represented by x_i , and n_{gas} , n_{DES} , $n_{co-solvent}$ and n_{Solid} indicate the number of moles of gas species, DES, co-solvent (water or EG), and solid particles in the liquid phase, respectively [82]. Assuming the gas phase contains a single component, the compressibility factor Z was calculated using the second virial coefficient method [83, 84].

To quantify the CO₂ capture from gas mixtures, gas samples were collected from the equilibrium cell once equilibrium between the gas and liquid phases was established. The gas composition was analyzed using a micro gas chromatograph (Varian 490 GC) equipped with molecular sieve 5A and Poraplot U columns, both connected to thermal conductivity detectors (TCD). The amount of each gas component (i) captured by the known mass of sorbent was then calculated based on its measured mole fraction in the gas phase and the corresponding equilibrium pressure, as expressed in Eq. (2-3).

$$n_i' = \frac{Y_i(p^{0,GR} - p^{eq,GR})V_{GR}}{RT} - \frac{y_i(p^{eq,EC} - p^s)(V_{EC} - V_s - V_r)}{RT} \quad (2-3)$$

where Y_i denotes the mole fraction of component i in the inlet gas stream, and y_i represents its mole fraction in the equilibrium gas phase, as determined by micro-GC analysis.

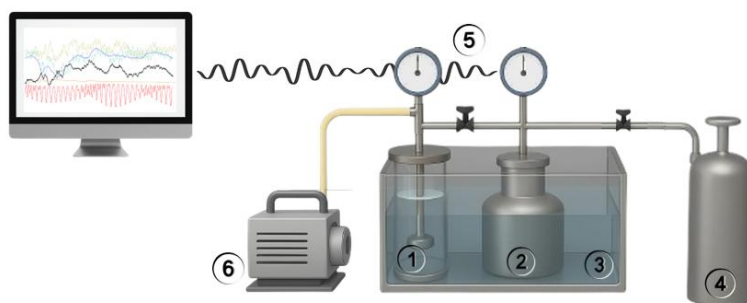


Fig. 2-2. Laboratory setup used for gas solubility measurements: 1. Equilibrium cell, 2. Gas reservoir, 3. Water bath, 4. Gas cylinder, 5. Pressure gauges, and 6. Vacuum pump.

2.4.2 CO₂ desorption

Desorption measurements: for the aqueous systems, desorption was performed at 100 °C and 1 bar using the experimental setup (similar to Fig. 2-1 (a)), which included a condenser and a drying tube (glass tube filled with silica gel) to minimize water loss during heating. In this case, N₂ gas was continuously purged into the system at a flow rate of 100 mL/min to facilitate CO₂ removal. In contrast, the non-aqueous systems underwent desorption at 110 °C and 1 bar without N₂ purging, where the CO₂-saturated samples were heated in an oil bath under continuous stirring. The desorbed amount was quantified by periodically weighing the samples using an analytical balance with a precision of ± 0.1 mg, until no further measurable mass loss was detected, indicating completion of the desorption process. Each sorption–desorption experiment was repeated three times, and the reported values represent the averages. The standard deviation of the measurements was within ± 0.07 wt.%.

2.5 Kinetics

The rate of CO₂ capture is a key factor in evaluating the overall efficiency of CO₂ capture systems. In this study, the kinetics of CO₂ capture were quantified using a kinetic model previously proposed in the literature [85, 86]:

$$r_p = -\frac{dC_{CO_2}}{dt} = K_a C_{CO_2} \quad (2-4)$$

where r_p , K_a , C_{CO_2} , and t are the CO₂ sorption rate (mol-CO₂/(kg-sorbent·min)), sorption rate constant (1/min), sorption amount (mol CO₂/kg sorbent), and time, respectively. Eq. (2-4) can be rewritten as follows:

$$\ln \frac{C_{CO_2}^t - C_{CO_2}^e}{C_{CO_2}^0 - C_{CO_2}^e} = -K_a t \quad (2-5)$$

where, $C_{CO_2}^t$, $C_{CO_2}^0$, and $C_{CO_2}^e$ represent the CO₂ capture (mol CO₂/kg sorbent) at time t , zero, and equilibrium, respectively. Assuming that the fresh solvent contains no CO₂ initially, $C_{CO_2}^0$ is taken as zero, and Eq. (2-5) can be rewritten as follows:

$$C_{CO_2}^t = C_{CO_2}^e (1 - e^{-K_a t}) \quad (2-6)$$

here $C_{CO_2}^t$ and $C_{CO_2}^e$ are determined from experimental measurements, while the sorption rate constant K_a is obtained by fitting the model to the experimental data.

Similarly, the CO₂ desorption rate and desorption rate constant were obtained using the kinetic model reported in previous studies [86, 87] as follows:

$$r_d = -\frac{d\beta}{dt} = k_d \beta \quad (2-7)$$

$$\beta_t = \beta_\infty + (\beta_0 - \beta_\infty)e^{-k_d t} \quad (2-8)$$

where r_d is the desorption rate of CO₂ (mol-CO₂/(kg-sorbent·min)) and k_d is the desorption rate constant (1/min), which was obtained from the fitting of the experimental values. β_t , β_∞ , and β_0 are the CO₂ concentrations in the solution (mol CO₂/kg absorbent) at time t , final equilibrium solution, and zero, respectively, which were obtained from the experimental measurements.

Chapter 3

3 Results and discussion

3.1 DES and substrate selection

3.1.1 Identification of DESs and further studies

In the initial stage of this thesis, a literature review and screening process were carried out to identify DESs with high CO₂ capture capacity, leading to the identification of several top-performing DESs reported in studies. DESs were prioritized for further investigation owing to their straightforward synthesis procedures and lower cost compared to ILs. Within this group, chemically reactive DESs were chosen for their superior selectivity toward CO₂. Based on factors such as cost and availability, a subset of these DESs was prepared in the laboratory to verify both reproducibility and capture performance. However, during capture experiments, these DESs demonstrated instability, with a noticeable decline in CO₂ uptake compared to initial reports. So, additional studies were undertaken to identify and develop a more stable DES.

In the search for alternatives to conventional MEA-based absorbents, Trivedi et al. [76] developed a series of DESs composed of [MEACl][EDA] with different molar ratios (1:1, 1:2, 1:3, and 1:4). Their results showed that these DESs exhibit improved corrosion resistance and lower heats of absorption compared with pure MEA and EDA. Among the investigated systems, [MEACl][EDA] demonstrated enhanced CO₂ capture, reaching up to 33.7 wt.%, while maintaining stable performance under humid conditions. In addition, the DES showed improved thermal stability and promising recyclability. Despite their favorable properties, these DESs exhibited a substantial increase in viscosity following CO₂ capture. Moreover, the addition of 10-30 wt.% water failed to alleviate

this issue, as the solutions tended to solidify after CO₂ capture, posing practical challenges for continuous operation. In this thesis, mixtures of [MEACl] and [EDA] with varying molar ratios were prepared and screened to identify DESs with improved performance.

To clearly distinguish DESs from conventional solvent mixtures, this thesis primarily relies on their thermodynamic non-ideality, which is evaluated using Eq. (3-1):

$$\ln(x_i\gamma_i) = \frac{\Delta_m h_i}{R} \left(\frac{1}{T_{m,i}} - \frac{1}{T_{m,m}} \right) \quad (3-1)$$

Here, x_i and γ_i represent the mole fraction and activity coefficient of the pure component i in the mixture, respectively, where the component can be either the HBD or HBA. $T_{m,i}$ and $\Delta_m h_i$ denote the melting point and melting enthalpy of the pure component i , while $T_{m,m}$ refers to the melting point of the mixture. R represents the universal gas constant.

According to Abranches and Coutinho [88], an activity coefficient (γ_i) value below unity ($\gamma_i < 1$) indicates a negative deviation from ideal behaviour, which is a characteristic of DES formation. Accordingly, Eq. (3-1) can be rearranged to determine the value of γ_i as follows:

$$\gamma_i = \frac{1}{x_i} \exp \left[\frac{\Delta_m h_i}{R} \left(\frac{1}{T_{m,i}} - \frac{1}{T_{m,m}} \right) \right] \quad (3-2)$$

In this thesis, the melting points ($T_{m,m}$) of [MEACl][EDA] mixtures with molar ratios of 1:3, 1:4.5, 1:5, 1:6, 1:7, and 1:10, along with that of the initial salt MEACl ($T_{m,MEACl}$), were determined using differential scanning calorimetry (DSC). The peak observed in the DSC graphs was used to identify the melting temperature (T_m). The measured $T_{m,MEACl}$ was 83.07 °C, consistent with the value reported by Trivedi et al. [76], with the melting points of the mixtures are summarized in Table 3-1. The

enthalpy of fusion for pure MEACl ($\Delta_m h_{MEACl}$) was obtained by integrating the corresponding DSC peak area. Besides, the melting point and enthalpy of fusion for pure EDA ($T_{m,EDA} = 10.95$ °C; $\Delta_m h_{MEACl} = 2108$ J/mol) were taken from the literature [89].

Using the molar ratios listed in Table 3-1, the corresponding mole fractions were calculated, and together with the measured $T_{m,m}$ and $\Delta_m h_i$ values, the activity coefficients γ_{EDA} and γ_{MEACl} were determined and summarized in the same table. The results showed that $\gamma_i < 1$ for mixtures with molar ratios of 1:3, 1:4.5, 1:5, and 1:6, indicating negative deviations from ideality, while mixtures with 1:7 and 1:10 ratios exhibited $\gamma_i > 1$. Consequently, [MEACl][EDA] systems with molar ratios between 1:3 and 1:6 were identified as DESs. In the work of Trivedi et al. [76], [MEACl][EDA] mixtures with ratios of 1:1, 1:2, 1:3, and 1:4 were also classified as DESs. By combining both sets of findings, it can be concluded that [MEACl][EDA] mixtures with molar ratios ranging from 1:1 to 1:6 exhibit the characteristics of DES.

Table 3-1. Melting point of mixtures ($T_{m,m}$) together with the activity coefficients of MEACl and EDA (γ_{MEACl} , γ_{EDA}) [90].

[MEACl][EDA] (HBA:HBD)	Melting point of			
	mixtures $T_{m,m}$ (°C)	γ_{MEACl}	γ_{EDA}	DES
(1:3)	-16.8	0.51	0.45	✓
(1:4.5)	-12.73	0.54	0.70	✓
(1:5)	-11.44	0.56	0.80	✓
(1:6)	-10.23	0.59	0.96	✓
(1:7)	-8.65	0.60	1.15	×
(1:10)	-5.43	0.64	1.74	×

Previous studies have frequently highlighted melting point depression as a key indicator for the formation of DES [91-93], with the melting point of the ideal solution ($T_{e,ideal}$) serving as a reference point. In this context, $T_{e,ideal}$ corresponds to the intersection of the solid-liquid equilibrium curves (x_i vs $T_{i,ideal}$) for MEACl and EDA, assuming ideal solution behavior. Based on Eq. (3-3), the solid-liquid equilibrium temperature of an ideal solution ($T_{i,ideal}$) for each component (MEACl and EDA) can be determined across different compositions (x_i):

$$T_{i,ideal} = \frac{T_{m,i}\Delta_m h_i}{\Delta_m h_i - RT_{m,i} \ln x_i} \quad (3-3)$$

Using Eq. (3-3), the $T_{i,ideal}$ values for both MEACl and EDA were calculated over the full composition range (0-1 mole fraction, x_i). The intersection of these two curves yielded the melting point of the ideal solution ($T_{e,ideal}$), determined to be 4.45 °C. Fig. 3-1 presents the melting points of all [MEACl][EDA] mixtures investigated in this study, together with those reported by Trivedi et al. [76], alongside the corresponding $T_{e,ideal}$ and the pure-component melting points of MEACl and EDA. As shown, all mixtures with molar ratios from 1:1 to 1:10 exhibit a pronounced decrease in melting temperature relative to both pure components and the ideal solution. This depression arises from the strong hydrogen bonding interactions between the HBD and HBA [94]. The observed deviation from $T_{e,ideal}$ further supports the formation of DESs, consistent with previous reports [95, 96]. Although the mixtures with molar ratios of 1:7 and 1:10 also exhibited melting points lower than $T_{e,ideal}$, they did not qualify as DES. This observation confirms that melting point depression alone can only serve as a qualitative indicator of DES formation, whereas thermodynamic non-ideality ($\gamma_i < 1$) can be considered as quantitative indicator. Consequently, subsequent investigations focused

on [MEACI][EDA] mixtures with molar ratios between 1:1 and 1:6, which were identified as DESs.

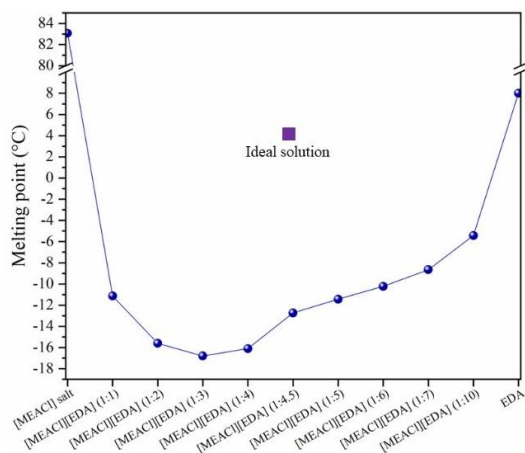


Fig. 3-1. Temperature-composition phase behavior for [MEACI][EDA] system [90].

3.1.2 Substrate selection

The choice of substrate was made based on insights gained from the literature review and preliminary screening. In recent years, significant attention has been devoted to developing solid sorbents through the incorporation of ILs or DESs into various supporting materials such as porous silica, zeolites, MOFs, activated carbon, alumina, and polymeric matrices. This strategy enables the immobilization of ILs or DESs, effectively mitigating challenges like high viscosity and cost by reducing the required amount of these liquids while retaining their advantageous properties.

A consistent trend observed across the literature is the predominant use of silica as the solid support for immobilization. This preference can be attributed to silica's affordability, wide availability, thermal and chemical stability, adjustable pore dimensions, and highly ordered porous

structure with a large surface area, the features that enable uniform dispersion of active sites and consequently enhance CO₂ uptake [97, 98]. In this thesis, silica was also chosen as the support material for DES immobilization.

3.2 Identification of the optimal aqueous DES

In this thesis, the optimal DES was determined based on two key parameters: CO₂ capture capacity and viscosity. These parameters are essential for evaluating the performance and practicality of a solvent in CO₂ capture applications. The aqueous DES that demonstrated a higher CO₂ capture capacity than the conventional MEA solution, while maintaining a viscosity similar to that of MEA, was selected as the optimal candidate.

3.2.1 CO₂ sorption performance

To verify the accuracy and reliability of the experimental setup, CO₂ capture measurements were first conducted at room temperature and atmospheric pressure, using a commercial 30 wt.% aqueous MEA solution. The obtained results were then compared with data reported in previous studies [99], showing strong consistency and confirming the validity of the experimental procedure.

Owing to the high viscosity of DESs with (1:1) and (1:2) molar ratios, CO₂ capture experiments were carried out only for ratios ranging from (1:3) to (1:6). The results obtained from the pure DESs revealed that the (1:3) DES solidified completely within 40 min of CO₂ exposure, while the (1:4) and (1:5) DESs formed gel-like substances, and the (1:6) DES produced a highly viscous product, which hindered further measurements and characterization. The DES with a (1:4.5) molar ratio exhibited a

comparable result to that of the (1:4) DES. To overcome the solidification, aqueous DES solutions containing 40–70 wt.% DES were prepared, where the DESs with (1:3), (1:4), (1:5), and (1:6) molar ratios were included.

The influence of water content and the [MEACl][EDA] molar ratio on CO₂ capture performance for these DESs is summarized in Fig. 3-2. The results demonstrated that increasing the EDA molar ratio from (1:3) to (1:6) led to an enhancement in CO₂ uptake, highlighting the effect of EDA concentration.

For all molar ratios, increasing the water content from 30 to 60 wt.% led to a noticeable decline in CO₂ capture capacity. This reduction can be attributed to the dilution of active sites and the decreased availability of functional groups [100, 101]. Interestingly, the aqueous [MEACl][EDA] DESs exhibited higher CO₂ capture capacity compared to aqueous MEA. In contrast, aqueous EDA showed higher CO₂ capture capacity than the aqueous DESs. However, Trivedi et al. [76] reported that it suffers from significant drawbacks, including higher corrosion rates relative to [MEACl][EDA], as well as issues related to flammability, volatility, and greater energy demands during solvent regeneration.

The CO₂ sorption of the 40 wt.% aqueous DES (1:5) system at room temperature and atmospheric pressure was selected as a representative example to illustrate the CO₂ uptake behavior over time, as shown in Fig. 3-2. The results revealed an initial rapid CO₂ capture during the first 10 min, followed by stabilization around 35 min, where the CO₂ uptake reached a steady-state value. This pronounced initial increase in CO₂ uptake can be attributed to the chemisorption mechanism facilitated by the [MEACl][EDA] system.

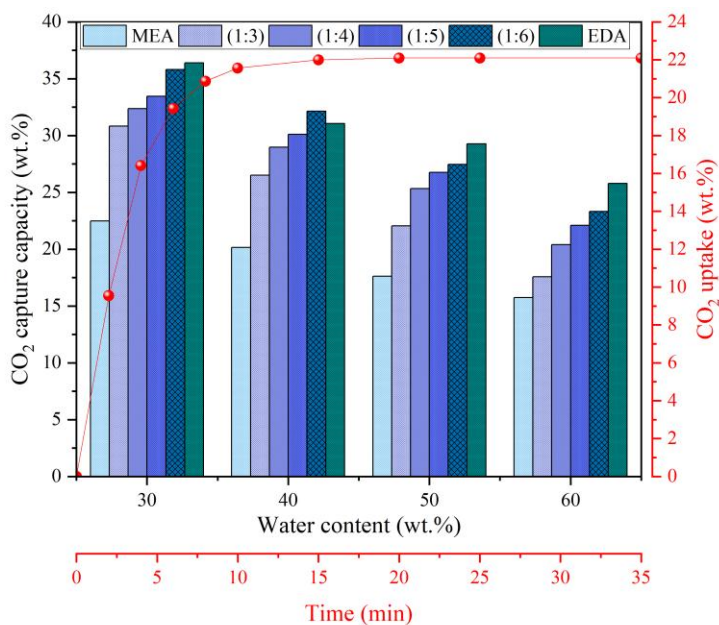


Fig. 3-2. CO₂ capture capacity of MEA, EDA, and DESs with (1:3) to (1:6) molar ratios as a function of water content together with CO₂ uptake of 40 wt.% aqueous DES (1:5) as a function of time [39, 90].

3.2.2 Viscosity

Viscosity, alongside CO₂ capture capacity, plays a critical role in governing mass transfer efficiency in absorption and desorption columns. Therefore, the viscosity of pure MEA, pure EDA, and [MEACI][EDA] DESs with molar ratios from (1:3) to (1:6), as well as their respective aqueous solutions, was evaluated before and after CO₂ capture.

The viscosities of pure MEA, pure EDA, and the synthesized DESs decreased steadily as temperature increased, as shown in Fig. 3-3 (a). With the exception of DES (1:3), all DES samples exhibited lower viscosities than MEA but remained more viscous than EDA. The influence of water is illustrated in Fig. 3-3 (b), where the aqueous forms of DES (1:3), (1:4),

and (1:5) displayed viscosity trends similar to MEA solutions, in which the addition of water consistently reduced viscosity over the entire concentration range. In contrast, aqueous DES (1:6) showed a viscosity pattern more comparable to that of aqueous EDA, with both increasing and decreasing fluctuations depending on water content. The impact of water content on viscosity was uniform across all tested temperatures from 20 to 50 °C. Furthermore, consistent with the behavior of the pure solvents, viscosity decreased with rising temperature in all aqueous systems.

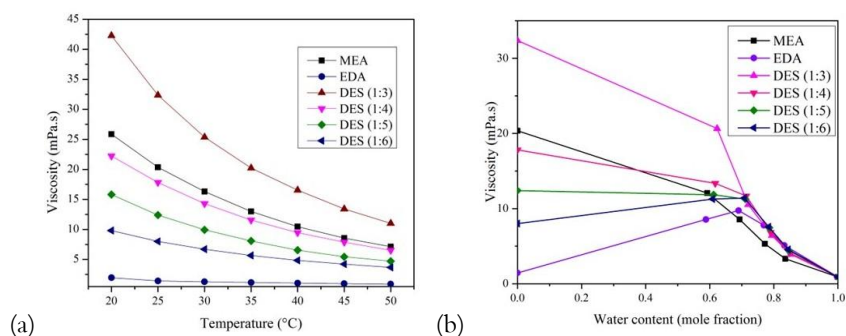


Fig. 3-3. Viscosity of (a) pure and (b) aqueous MEA, EDA, and [MEACl][EDA] with (1:3), (1:4), (1:5), and (1:6) molar ratios as a function of temperature and water content at 25 °C, respectively, before CO₂ capture [39, 90].

After CO₂ capture, solidification or gel formation was observed in pure and some of the aqueous samples. Pure EDA and its aqueous samples containing 30 and 40 wt.% water, as well as the pure DES with a (1:3) molar ratio, fully solidified. In addition, all DESs with 30 wt.% water developed gel-like structures following CO₂ capture. Consequently, viscosity could not be measured for these samples. For the remaining aqueous systems, increasing the water content significantly reduced viscosity after CO₂ capture. The influence of water content on viscosity

remained consistent across the entire temperature range of 20–50 °C, and as expected, viscosity decreased with increasing temperature.

After CO₂ capture, a clear increase in viscosity was observed compared to the original solvent systems, as shown in Figs. 3–4 (a–c), with the effect being more pronounced at lower temperatures and higher DES concentrations. This trend is consistent with previous reports on chemically reactive absorbents, including systems such as [ChCl][EG/HMDA], [ChCl][EG/AEEA], [ChCl][EG/MAPA], [ChCl][EG/EDA], [ChCl][EG/BDA] [102], and [ChCl][MEA] [103].

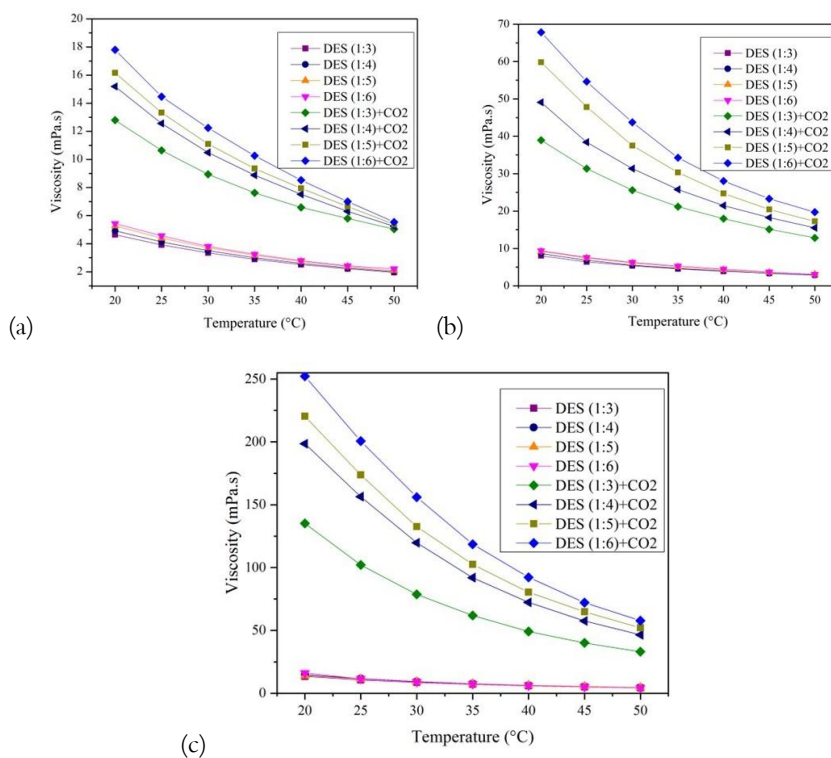


Fig. 3-4. Viscosity of aqueous [MEACl][EDA] with (1:3), (1:4), (1:5), and (1:6) molar ratios in (a) 40 wt.%, (b) 50 wt.%, and (c) 60 wt.% DES concentration before and after CO₂ capture as a function of temperature [39, 90].

From the results presented in Sections 3.2.1 and 3.2.2, the samples containing 40 wt.% [MEACl][EDA] with (1:5) molar ratio was identified as the preferred candidate. This formulation demonstrated a relatively high CO₂ capture capacity of 22.09 wt.% while maintaining a manageable viscosity of 4.401 mPa·s before and 13.330 mPa·s after CO₂ capture at 25 °C, which is comparable to aqueous MEA with viscosities of 3.318 and 8.413 mPa·s before and after absorption, respectively (15.74 wt.% CO₂ capture capacity). Therefore, this optimal sample was selected for further investigations.

3.2.3 FTIR analysis

FTIR spectra were recorded for the pure DES, as well as its aqueous solution before/after CO₂ capture, as illustrated in Fig. 3-5. The absorption band between 3000 and 3600 cm⁻¹ is associated with the stretching vibrations of OH and NH groups originating from MEA and EDA [104]. Bands detected at ~2850 and 2930 cm⁻¹ correspond to the CH₂ stretching modes of these amine components [104, 105]. Additional characteristic peaks at 1645, 1470, and 1070 cm⁻¹ are assigned to NH bending in primary amines, CH₂ group vibrations, and CN stretching, respectively [104].

A comparison of the spectra of pure DES and its aqueous one before CO₂ capture reveals a noticeable broadening within the 3000–3600 cm⁻¹ region. This broadening arises from overlapping OH stretching bands of water molecules and the hydrogen-bonding interactions inherent to the DES structure [106, 107], in agreement with observations reported for a 75 vol.% aqueous [ChCl][MEA] (1:5) DES [107].

After CO₂ capture, the disappearance of the NH stretching band near 3290 cm⁻¹ indicates the participation of amine groups in carbamate formation. Furthermore, the appearance of a new band at around 1185 cm⁻¹ is attributed to symmetric C–O stretching vibrations [76, 108]. The emergence of a band in the 1300–1340 cm⁻¹ region is also consistent with vibrations associated with carbamate species, including contributions from C=O and C–O groups [109, 110].

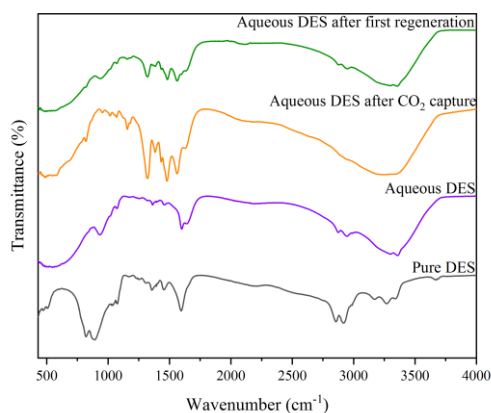


Fig. 3-5. FTIR spectra of pure DES before CO₂ capture and 40 wt.% aqueous [MEACl][EDA] (1:5) before and after CO₂ capture and after first regeneration [39, 90].

3.2.4 Effect of temperature on CO₂ capture capacity

The influence of temperature on the CO₂ capture performance of the selected DES solution was investigated within a temperature range of 5–80 °C. As shown in Fig. 3-6, CO₂ uptake decreased markedly with increasing temperature. The highest capture capacity, 25.12 wt.%, was obtained at 5 °C, whereas a substantial decline to 3.15 wt.% was observed at 80 °C. This reduction in capture capacity at elevated temperatures is attributed to the weakened driving force for CO₂ uptake. Similar

temperature-dependent behavior reported in previous studies confirms the inhibitory effect of higher temperatures on CO₂ uptake [111, 112].

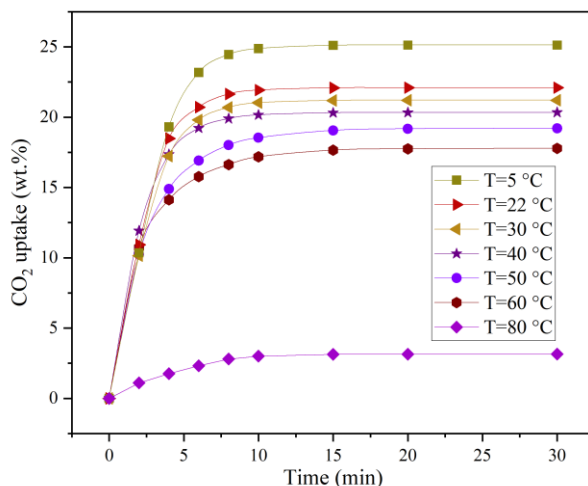


Fig. 3-6. Effect of temperature on the CO₂ uptake of 40 wt.% aqueous [MEACl][EDA] (1:5) [39, 90].

3.2.5 Absorption-desorption cyclic performance

To assess the potential of the synthesized DES for practical and industrial applications, its reusability was examined through consecutive absorption-desorption cycles. The most noticeable decline in CO₂ capture capacity occurred during the first regeneration step, with a reduction of ~10.08%. In the following cycles, only a slight decrease in performance was observed, indicating good stability of the solvent system. After five repeated cycles, the CO₂ capture capacity reached 19.44 wt.%, corresponding to a retention of ~88% of the initial uptake.

To examine the structural stability of the DES after regeneration, FTIR analysis was performed on the aqueous DES following the first desorption cycle, as shown in Fig. 3-5. The spectra indicate that the main

functional structure of the DES was preserved after regeneration, with only minor changes detected. The NH stretching band at 3290 cm^{-1} , which had disappeared after CO_2 capture due to carbamate formation, reappeared after regeneration, confirming partial recovery of amine groups. However, the bands observed at $1300\text{--}1340\text{ cm}^{-1}$ and around 1185 cm^{-1} showed a noticeable decrease in intensity, suggesting that although most of the chemisorbed CO_2 was released, a fraction of CO_2 molecules remained bound to the DES. This residual interaction is likely responsible for the slight decline in CO_2 capture capacity during repeated cycles. Comparable trends have been reported for other DES systems such as Im-MEA and [ChCl][MEA], as noted by Shi et al. [113] and Huan et al. [114].

3.2.6 Kinetics

Based on the experimental CO_2 uptake data and the theoretical approach described in Section 2.5, the absorption rates and corresponding rate constants were determined for the 40 wt.% aqueous [MEACl][EDA] (1:5) system at temperatures ranging from 20 to 50 °C, as well as for a 40 wt.% aqueous MEA at room temperature (22 °C). The calculated values are presented in Table 3-2. Aqueous MEA was included in the analysis to provide a benchmark for comparison with the DES-based system.

The absorption rate constants (K_a) were determined by fitting the experimental data to Eq. 2-6, and the resulting values (mean values) are summarized in Table 3-2 with $R^2 > 0.98$ and standard deviation of ± 0.01 1/min. The K_a value obtained for the conventional aqueous MEA was lower than that of the aqueous DES developed in this thesis, indicating a slower CO_2 uptake process for MEA. Absorption rates depicted that the DES showed an increase in rate with temperature from 5 to 40 °C,

reaching a maximum at 40 °C, after which the rate declined as the temperature rose further to 80 °C. Comparison of the kinetic behavior revealed that MEA required a longer time to reach equilibrium, whereas the DES showed a faster CO₂ uptake.

Table 3-2. Absorption rate and absorption rate constant (K_a) of 40 wt.% aqueous [MEACl][EDA] (1:5) across 5-80 °C and 40 wt.% aqueous MEA at 22 °C [39, 90].

Temperature (°C)	K_a (1/min)	Maximum rate (mol-CO ₂ /(kg-sorbent·min))
40 wt.% MEA		
22	0.22	0.70
40 wt.% [MEACl][EDA] (1:5)		
5	0.34	1.18
22	0.40	1.24
30	0.44	1.27
40	0.46	1.35
50	0.37	1.16
60	0.35	1.12
80	0.22	0.13

3.3 Integration of immobilization and co-solvent addition

This section describes the development of a slurry system by combining immobilization techniques with co-solvent addition to enhance CO₂ capture performance. In this approach, the DES was first immobilized onto a solid support, and the resulting composite was subsequently blended with the aqueous DES selected in the previous section. Afterwards, the work was extended to non-aqueous systems by using EG as a co-solvent.

3.3.1 Structural characteristics of immobilized DES

The textural properties of the DES-immobilized silica samples were examined using nitrogen adsorption-desorption analysis. Given the slight variations observed across the tested range, the structural assessment focused on samples containing 3, 5, and 15 wt.% DES loadings (Table 3-3). The unmodified silica exhibited the highest surface area, which progressively decreased as the DES content increased from 3 to 15 wt.%. A comparable declining trend was also observed in pore diameter and pore volume. These changes indicate the successful confinement of DES molecules within the silica pores.

Table 3-3. Surface area, pore size, pore volume, and estimated DES layer thickness of *x*-DES@silica [81].

Sample	BET surface area (m ² /g)	Average pore diameter (nm)	Total pore volume (cm ³ /g)	DES layer thickness (nm)*	Pore occupancy (%)
Silica	710.80	12.31	1.78	0	0
3-DES@silica	400.58	10.17	1.26	0.72	29
5-DES@silica	385.15	9.93	1.18	0.83	33
15-DES@silica	357.94	9.77	1.15	0.88	35

* Thickness of DES layer = $(V_{pore,support} - V_{pore,DES})/BET_{support}$ [115].

3.3.2 Aqueous slurry

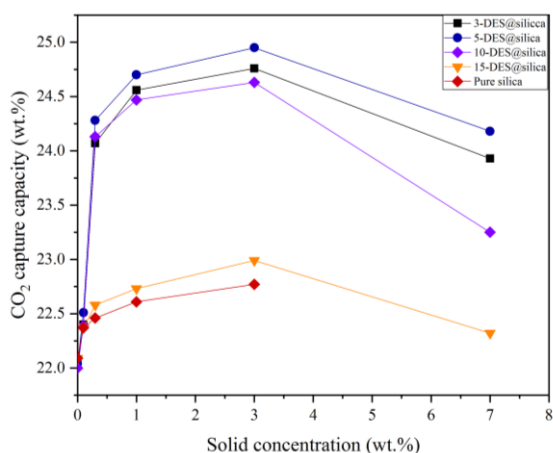
3.3.2.1. CO₂ sorption measurements

The CO₂ capture capacity was determined for slurries prepared by incorporating 0-7 wt.% of *x*-DES@silica (*x* = 3, 5, 10, and 15 wt.%) into the optimized aqueous DES system. Among them, the slurry exhibiting

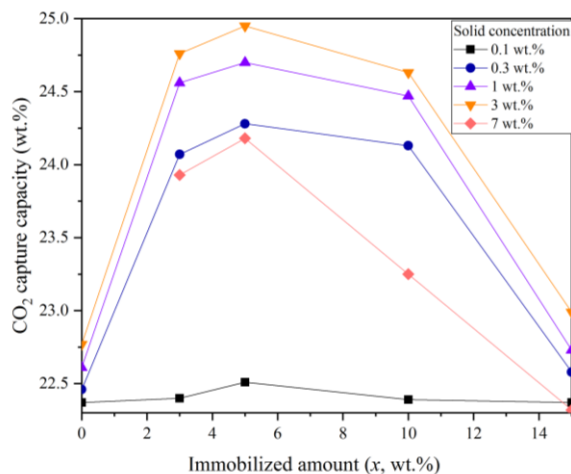
the highest CO₂ capture capacity was selected for additional characterizations.

The effect of *x*-DES@silica concentration (0.1–7 wt.%) in aqueous DES is summarized in Fig. 3-7 (a). Increasing the concentration of immobilized DES particles (e.g., 3-DES@silica) from 0 to 3 wt.% enhanced the CO₂ capture capacity, reaching a maximum of 24.76 wt.%. However, further addition beyond 3 wt.% led to a decline in CO₂ capture capacity (to 23.93 wt.%). This trend was consistent across all systems (5-, 10-, and 15-DES@silica), indicating an optimal loading of 3 wt.% in the aqueous DES. The initial enhancement in CO₂ uptake is attributed to improved gas–liquid mass transfer, resulting from bubble fragmentation due to particle collisions and suppression of bubble coalescence, which increases the interfacial area [65–67]. At higher solid loadings, however, excessive particle coverage around gas bubbles hinders mass transfer, while particle aggregation reduces the effective surface area [68]. Moreover, all slurries containing *x*-DES@silica exhibited higher CO₂ capture capacities (up to 24.93 wt.%) compared to both aqueous DES (22.09 wt.%) and slurries containing pure silica (22.77 wt.%). This improvement is attributed to the additional CO₂ sorption provided by the functionalized porous particles. At solid loadings above 3 wt.% (for pure silica), a mud-like, highly viscous system was observed. The increased viscosity limits CO₂ diffusion and mass transfer, reducing capture efficiency. Additionally, such rheological behavior poses practical challenges in handling and pumping, potentially increasing operational costs and complicating process design. This behavior aligns with previous studies [116–118], which reported that at higher solid concentrations, particle aggregation occurs, reducing the available surface area for CO₂ interaction.

The effect of immobilization loading (x) in x -DES@silica ($x = 0, 3, 5, 10, \text{ and } 15 \text{ wt.}\%$) on the CO_2 capture capacity of the slurries is presented in Fig. 3-7 (b). The CO_2 capture capacity increased with increasing DES immobilization up to 5 wt.%, after which a decline was observed. This decrease at higher loadings ($x > 5 \text{ wt.}\%$) is attributed to reductions in surface area, pore volume, and pore size of the material. Similar trends have been reported in previous studies, highlighting the influence of DES film thickness on CO_2 capture, where thinner films facilitate higher uptake [119-121]. At lower loadings, increasing DES content provides more active sites for CO_2 interaction, enhancing capture capacity compared to pure silica. However, excessive DES loading leads to reduced surface accessibility, thereby limiting CO_2 sorption. These findings indicate that CO_2 capture performance is governed by a trade-off between surface chemistry (availability of active sites) and structural properties (porosity and surface area). The highest CO_2 capture capacity (24.93 wt.%) was achieved for the slurry containing 3 wt.% of 5-DES@silica in aqueous DES. This composition was therefore selected as the optimal system for further characterization.



(a)



(b)

Fig. 3-7. CO₂ capture capacity of slurries made by the incorporation of 0-7 wt.% of (*x*-DES@silica, *x* = 0-15 wt.%) into the aqueous DES, as a function of (a) solid concentration and (b) immobilization amount [39, 81].

3.3.2.2. Effect of temperature

As shown in Fig. 3-8, a decline in CO₂ capture capacity was observed with increasing temperature, consistent with the trend observed in the aqueous DES system. The maximum CO₂ capture capacity of 25.33 wt.% was recorded at 5 °C, which decreased substantially to 7.71 wt.% at 80 °C. Although lower temperatures favored higher CO₂ capture capacity, the rate of CO₂ uptake was notably slower under these conditions.

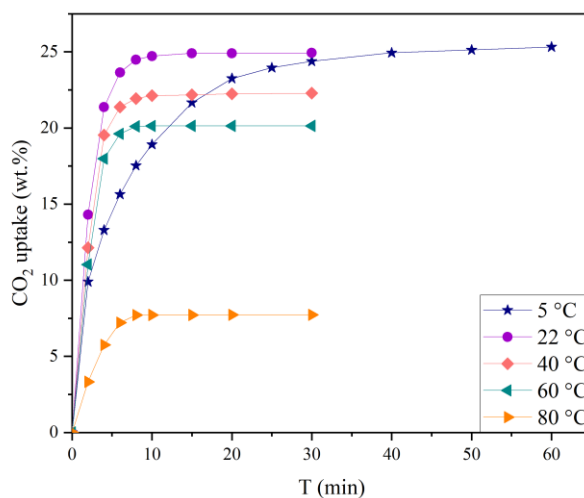


Fig. 3-8. Effect of temperature on CO₂ uptake of the aqueous slurry [39, 81].

3.3.2.3. Viscosity

Fig. 3-9 presents the viscosity profile of the slurry before and after CO₂ capture. Before CO₂ capture, the slurry exhibited its maximum viscosity of 7.9 mPa·s at 20 °C, which gradually declined to 4.3 mPa·s as the temperature rose to 50 °C. Compared with the aqueous DES, the slurry showed higher viscosity values. Additionally, relative to the slurry prepared with pure silica (6.3–3.1 mPa·s across 20–50 °C), the system containing immobilized silica demonstrated a slightly higher viscosity. This increase can be ascribed to the intermolecular interactions introduced by the immobilized silica in the slurry. Nevertheless, the viscosity of the immobilized silica-based slurry remained relatively low (<7.9 mPa·s), comparable to that of the aqueous system (<5.3 mPa·s).

After CO₂ capture, the viscosity rose to 23.0 mPa·s at 20 °C and gradually decreased to 12.3 mPa·s as the temperature increased to 50 °C. The slurry containing immobilized silica showed a higher viscosity,

displaying a more distinct deviation compared to both the aqueous DES and the slurry with pure silica. This increase can be attributed to the enhanced CO₂ uptake by the solid phase of the slurry. In particular, the silica particles functionalized with DES offered additional active sites for CO₂ uptake.

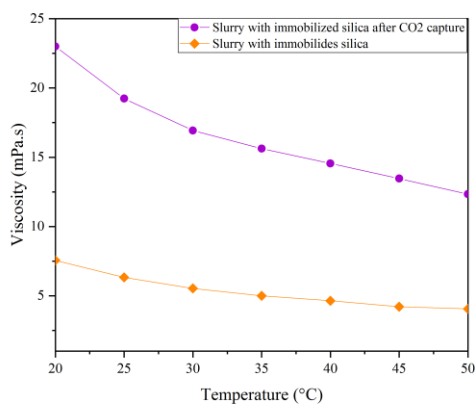


Fig. 3-9. Viscosity of the aqueous slurry before and after CO₂ capture.

3.3.2.4. Stability

Maintaining long-term stability is essential for the sustained performance of CO₂ capture systems. To evaluate this aspect, the slurry was stored at room temperature (22 °C) and then the CO₂ capture capacity of the slurry (containing 3 wt.% of 5-DES@silica in aqueous DES) was measured over different time intervals. The results revealed that the slurry maintained consistent CO₂ capture behavior throughout the testing period. Notably, the CO₂ capture capacity showed only a slight decline from 24.93 to 24.80 wt.% after one month, corresponding to a minor reduction of 0.48%.

3.3.2.5. FTIR analysis

Fig. 3-10 presents the FTIR spectra of 5-DES@silica, pure silica, aqueous DES, and the corresponding slurries containing pure and immobilized silica. Several new peaks emerged after the immobilization process. Notably, peaks in the 1450-1630 cm^{-1} region correspond to the NH_2 vibrations of RNH_2 groups [122-124], while the band near 2948 cm^{-1} is associated with CH_2 stretching vibrations [125, 126], suggesting the successful incorporation of DES within the silica framework. The characteristic peaks at 455, 800, and 1098 cm^{-1} are attributed to the asymmetric stretching and bending of Si-O-Si bonds [127, 128], whereas those at 1635 and 970 cm^{-1} are corresponded to Si-OH vibrations [129]. Furthermore, an absorption band around 3700 cm^{-1} describe the presence of hydroxyl groups, likely originating from adsorbed water molecules [130].

The characteristic peaks of the aqueous DES correspond well with those reported by Trivedi et al. [76] and with our earlier findings [90] presented in Section 3.2.3. The retention of these signature peaks after introducing both pure silica and immobilized silica particles confirms that the structural integrity of the DES was maintained. Additionally, the enhanced intensity of the peaks at 1410 and 1230 cm^{-1} [131], attribute to C-N stretching, and at 1580 cm^{-1} , associate with NH_2 vibrations [123], suggests an increased presence of DES resulting from the incorporation of immobilized DES.

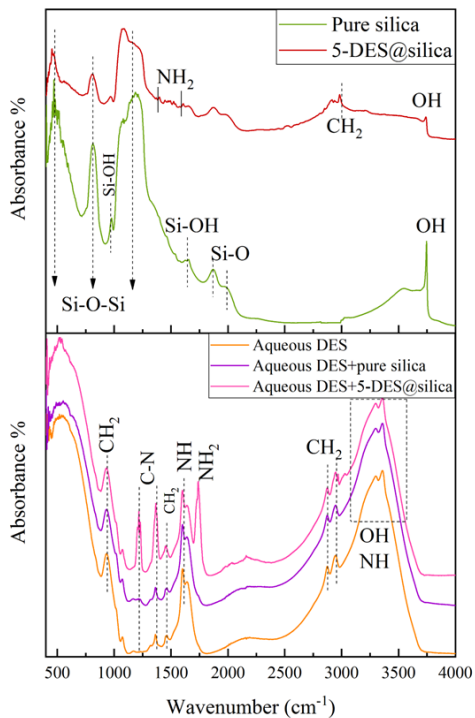


Fig. 3-10. FTIR spectra of pure silica, 5-DES@silica, aqueous DES, and slurries prepared by pure silica and 5-DES@silica [39].

3.3.2.6. Cyclic performance

The regeneration of the slurry through multiple cycles of sorption and desorption was studied and the findings showed that the slurry containing 3 wt.% of 5-DES@silica in aqueous DES achieved its highest CO₂ capture capacity of 24.93 wt.% during the first cycle, which gradually decreased to 22.73 wt.% after five cycles. The most notable decline (~8.82%) occurred during the initial regeneration step, with ~91% of the original CO₂ capture capacity retained after five sorption-desorption cycles (Fig. 3-11). When compared with the aqueous DES, the slurry

consistently demonstrated higher CO₂ capture capacity across repeated cycles, despite a gradual reduction in capture efficiency for both systems.

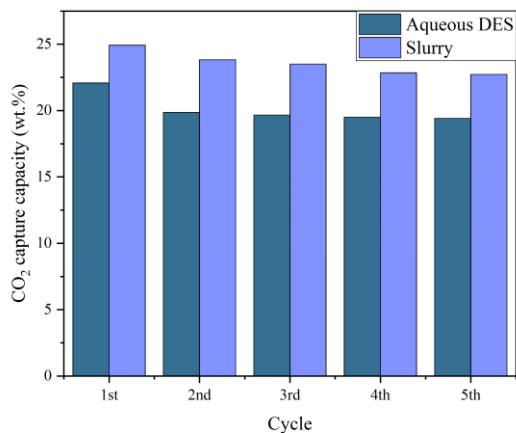


Fig. 3-11. Recycling performance of the aqueous slurry (aqueous DES performance is added for comparison) [39, 81].

3.3.2.7. Kinetics

Based on both the experimental CO₂ uptake results and the theoretical model outlined in Section 2.5, the sorption rates of the slurry and the corresponding rate constants (K_a) were calculated across different temperatures. K_a values were obtained by fitting the experimental data to Eq. 2-6 and average values of three independent measurements, with standard deviation of ± 0.01 1/min are summarized in Table 3-4.

Consistent with the trend observed for aqueous DES (Table 3-2), the data in Table 3-4 indicate that the sorption rate constant increased from 22 to 40 °C, then gradually declined as the temperature rose to 80 °C. Moreover, the sorption rate constant for CO₂ uptake using the slurry at

22 °C was higher than that of the aqueous DES under the same conditions.

Table 3-4. Sorption rate constant (K_s) and sorption rates (r_s) of slurry at 5 to 80 °C and 40 wt.% aqueous [MEACl][EDA] (1:5) at 22 °C [81].

Temperature (°C)	K_s (1/min)	Maximum rate (mol-CO ₂ /(kg-sorbent·min))
40 wt.% [MEACl][EDA] (1:5)		
22	0.40	1.24
Slurry		
5	0.16	1.13
22	0.46	1.38
40	0.48	1.63
60	0.42	1.13
80	0.35	0.38

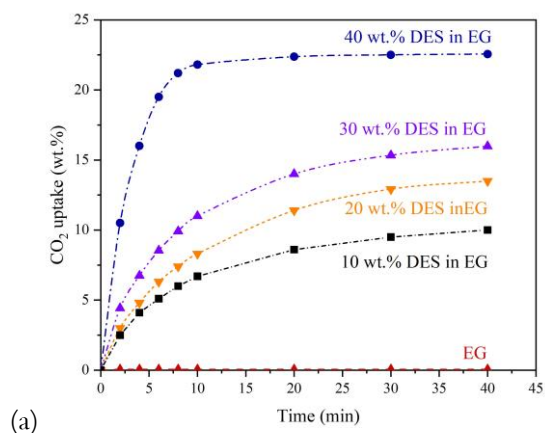
3.3.3 Non-aqueous slurry

3.3.3.1. CO₂ sorption measurements

Before the preparation and study of the slurry, non-aqueous DESs were prepared by initially mixing the DES with EG as the co-solvent. Similar to aqueous slurry, different DES concentrations (0–40 wt.%) in the co-solvent were prepared and subjected to CO₂ capture at 22 °C and 1 bar (Fig. 3-12 (a)). A maximum uptake of 22.56 wt.% was achieved at 40 wt.% DES, which decreased to 15.98, 13.50, and 10.00 wt.% for 30, 20, and 10 wt.% DES, respectively. Pure EG showed negligible CO₂ uptake (~0.05 wt.%). On the other hand, despite the higher capture capacity at 40 and 30 wt.% DES, their high viscosities (1120.341 and 540.152 mPa·s at 22 °C, respectively) hindered processability; therefore, 20 wt.% DES in EG was selected as the optimal composition with

135.220 mPa·s at 22 °C, offering a balance between CO₂ capture capacity and manageable viscosity.

Subsequently, in accordance with the optimized solid concentration and immobilization loading identified in the previous section, 3 wt.% of immobilized silica (5-DES@silica) was incorporated into the 20 wt.% DES in EG mixture (Fig. 3-12 (b)). The addition of both pure and immobilized silica improved the CO₂ capture capacity, reaching maximum uptakes of 14.20 and 15.02 wt.%, respectively. Similar to the aqueous slurries, this enhancement can be attributed to the presence of solid particles, which provide additional sorption sites by increasing the available surface area for CO₂ interaction. Moreover, immobilizing DES onto silica combines the chemical affinity of DES with the high surface area and porosity of the support.



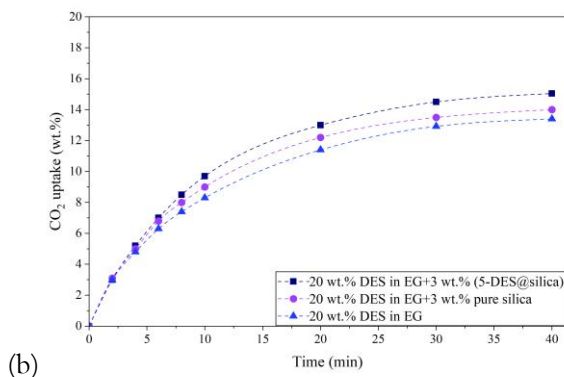


Fig. 3-12. CO₂ uptake of (a) pure EG and DES in EG mixtures with various concentrations and (b) non-aqueous slurries made by the addition of 3 wt.% pure and 5-DES@silica [77].

The effect of temperature on the non-aqueous system was also investigated, and the results are presented in Fig. 3-13. As expected, an increase in temperature led to a systematic reduction in CO₂ capture capacity, consistent with trends observed for the aqueous slurry. The maximum uptake of 16.03 wt.% was obtained at 5 °C, which gradually decreased to 6.30 wt.% at 80 °C, demonstrating the inverse relationship between temperature and capture capacity. At elevated temperatures, reduced viscosity enhances mass transfer and accelerates the approach to equilibrium; however, this occurs at the expense of lower CO₂ capture capacity.

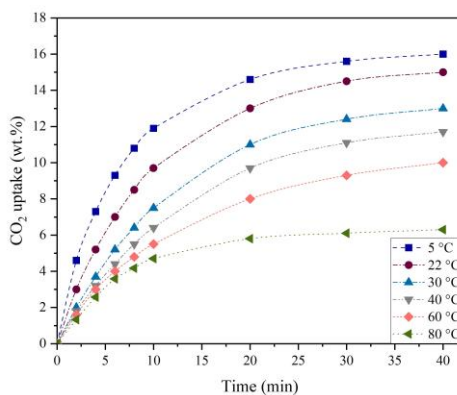


Fig. 3-13. Effect of temperature on CO₂ uptake of the non-aqueous slurry [77].

3.3.3.2. Viscosity

The viscosity of the non-aqueous system was evaluated before and after CO₂ capture over a temperature range of 20–50 °C (Fig. 3-14). Prior to CO₂ capture, the addition of 3 wt.% pure silica and 5-DES@silica led to a moderate increase in viscosity across all temperatures, which can be attributed to physical interactions between the solid particles and the liquid phase, consistent with observations in the aqueous slurry [77].

After CO₂ capture, a substantial increase in viscosity was observed for all systems. This increase is primarily associated with carbamate formation during CO₂ sorption. Among all samples, the 5-DES@silica slurry showed the highest viscosity, which decreased from 284.3 mPa·s at 20 °C to 38.2 mPa·s at 50 °C. In all cases, viscosity decreased significantly with increasing temperature, highlighting the strong temperature dependence of the system's rheological behavior [77].

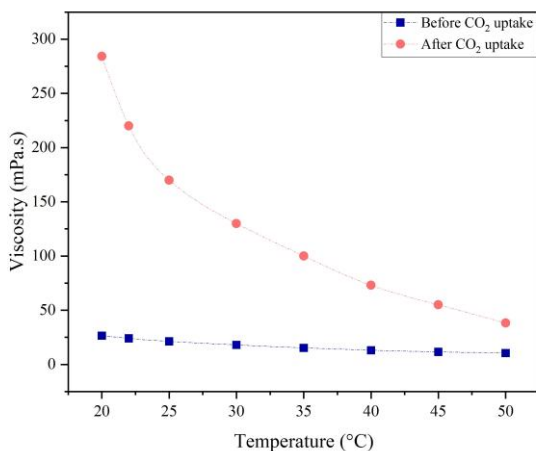


Fig. 3-14. Viscosity of the non-aqueous slurry before and after CO₂ capture [77].

3.3.3.3. Stability

To evaluate the performance of the slurry after a long time, it was stored for one month at room temperature, after which its CO₂ capture capacity was re-evaluated. Similar to the aqueous slurry, the results showed only a negligible reduction in CO₂ uptake, with no significant change in the capture profile, indicating good stability over time.

3.3.3.4. FTIR analysis

The CO₂ uptake of the non-aqueous slurry was further investigated using FTIR analysis before and after CO₂ capture, as shown in Fig. 3-15. Prior to CO₂ sorption, the spectra confirmed the presence of characteristic functional groups of both EG and DES, indicating that the addition of silica did not alter the chemical structure of the components. Upon mixing DES with EG, the band in the 3000–3600 cm⁻¹ region became broader, indicating the combined contributions of OH and NH groups from EDA and MEA in the DES [51, 104]. An increase in NH

peak intensity upon silica addition suggested effective immobilization of DES on the silica surface [77].

Similar to the aqueous slurry, after CO₂ capture, new peaks appeared at 1400–1550 cm⁻¹, corresponding to carbamate formation, confirming chemical interaction between CO₂ and amine groups in the DES. This was further supported by the reduction of NH-related bands, indicating their involvement in the reaction. Additionally, a peak associated with carbonate species suggested minor interaction between EG and CO₂. Overall, the results demonstrate that CO₂ capture in the slurry is primarily governed by chemisorption through DES, with a minor contribution from EG, consistent with previous studies.

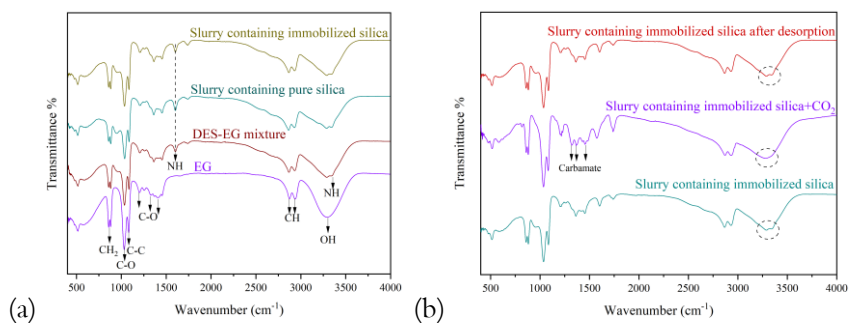


Fig. 3-15. FTIR spectra of (a) EG, DES-EG mixture, and non-aqueous slurry before CO₂ sorption and (b) non-aqueous slurry after CO₂ sorption and after desorption [77].

3.3.3.5. Cyclic performance

The cyclic stability of the developed slurry was evaluated over five consecutive sorption-desorption cycles. CO₂ sorption was performed at 22 °C and 1 bar, followed by desorption at 110 °C under continuous stirring. Similar to the aqueous slurry, the results showed a slight decline in CO₂ capture capacity from 15.02 wt.% in the first cycle to 14.46 wt.% in the fifth, corresponding to a high retention of 96.4%. CO₂ uptake was

initially completed within ~30 min and gradually increased to ~40 min in later cycles, while desorption time also slightly increased with cycling. Similar to aqueous slurry, the minor reduction in performance was attributed to residual CO₂ remaining after regeneration. FTIR analysis after desorption confirmed the reversibility of the process, as carbamate-related peaks disappeared and NH bands reappeared, indicating preservation of the chemical structure during repeated use [77].

3.3.3.6. Kinetics

The apparent CO₂ sorption rates and corresponding rate constants were determined over a temperature range of 5–80 °C by fitting the experimental data to the equations described in section 2.5. The average values of the sorption and desorption rates and rate constants were subsequently analyzed and are summarized in Table 3-5. Both the maximum sorption rate and rate constant decreased with increasing temperature, dropping from 0.52 to 0.15 mol-CO₂/(kg-sorbent·min) and from 0.14 to 0.08 1/min, respectively, due to reduced driving force despite lower viscosity. In comparison, the slurry exhibited higher sorption rates and rate constants than the corresponding DES-EG mixture, highlighting the positive effect of solid particles on enhancing kinetics. These findings are consistent with trends observed in similar aqueous systems.

Table 3-5. Sorption/desorption rate constants (K_a , K_d) and maximum sorption/desorption rates (r_a , r_d) of 20 wt.% DES in EG mixture and the non-aqueous slurry at various temperature and 1 bar [77].

Sorption temperature (°C)	K_a (1/min)	Maximum rate (r_a)	Desorption temperature (°C)	K_d (1/min)	Maximum rate (r_d)
DES-EG mixture					
22	0.07	0.27	110	0.10	0.30
Slurry					
5	0.14	0.52			
22	0.11	0.34			
30	0.09	0.25			
40	0.08	0.20	110	0.18	0.38
60	0.08	0.18			
80	0.08	0.15			

3.4 Further studies

3.4.1 CO₂ sorption using pure CO₂ and synthetic gas mixtures

Prior to measuring the CO₂ capture capacity from pure CO₂ and synthetic gas mixtures in the gas-liquid equilibrium apparatus (VLE), the experimental setup was validated by measuring the CO₂ capture capacity of H₂O and EG. The obtained results were in good agreement with literature data, confirming the accuracy and reliability of the experimental system.

(a) Pure gas measurements: The CO₂ capture capacity in the developed aqueous and non-aqueous slurries was evaluated at 30 °C over a range of pressures, with the results summarized in Figs. 3-16 (a) and (b).

As shown in Fig. 3-16, the addition of 3 wt.% pure silica to the DES enhances CO₂ capture capacity across the entire pressure range, with a more pronounced effect observed for the aqueous slurry. This enhancement is primarily attributed to CO₂ physisorption through van der Waals interactions. Similar trends have been reported in previous studies, where the incorporation of solid adsorbents (e.g., silica) into liquid amine or DES solvents resulted in absorption–adsorption slurries with improved overall CO₂ capture capacity [39]. Immobilizing silica particles with the same DES (5-DES@silica) produced the most significant enhancement for both aqueous and non-aqueous slurries. This can be attributed to the combined effects of chemical absorption by DES and physisorption on the high-surface-area silica.

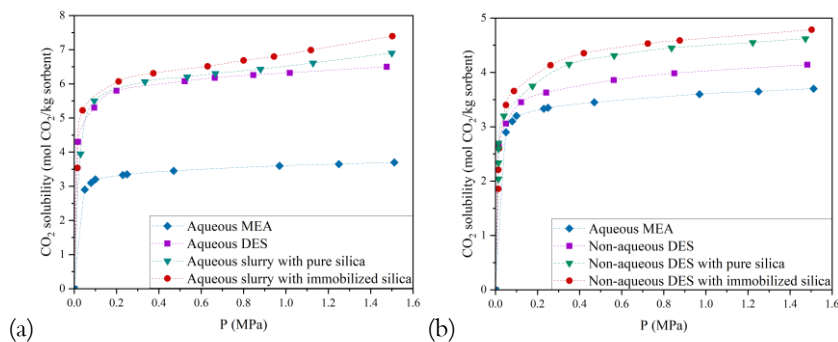


Fig. 3-16. CO₂ solubility of the developed (a) aqueous and (b) non-aqueous slurries together with 40 wt.% aqueous DES, 20 wt.% non-aqueous DES, and 30 wt.% aqueous MEA at 30 °C as the function of pressure using pure CO₂.

(b) Gas mixture measurements: To simulate industrial biogas conditions, a synthetic gas mixture containing 40% CO₂ and 60% CH₄ was employed to evaluate the CO₂ capture capacity of the developed aqueous and non-aqueous slurries at 30 °C. The corresponding results are presented in Figs. 3-17 (a) and (b). In both systems, the presence of CH₄ had a negligible effect on CO₂ capture capacity, indicating that CH₄ behaved as an inert component under the investigated conditions. Consistent with the pure CO₂ results, the incorporation of solid phases, either pure silica or DES-immobilized silica, enhanced the CO₂ capture capacity in both aqueous and non-aqueous slurries compared to their solid-free counterparts. While the aqueous slurry exhibited negligible CH₄ uptake, the non-aqueous slurry containing EG showed higher CH₄ sorption. This behavior can be attributed to the higher uptake of CH₄ in EG and its physical adsorption on silica surfaces.

Similarly, Figs. 3-18 (a) and (b) depict the CO₂ capture behavior of the aqueous and the non-aqueous system in the presence of a CO₂/N₂ gas mixture. In both cases, CO₂ capture capacity increased at low pressures and subsequently approached a plateau as pressure increases, reflecting a strong affinity between CO₂ and the DES. In contrast, N₂ uptake remains negligible across the entire pressure range. The incorporation of solid phases further enhances CO₂ capture performance: pure silica leads to a moderate increase in CO₂ solubility, whereas immobilized silica consistently achieves the highest capture capacity.

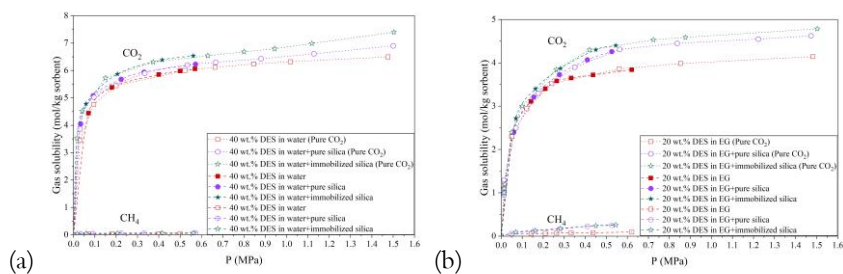


Fig. 3-17. Gas solubility of the developed (a) aqueous and (b) non-aqueous slurries at 30 °C as the function of pressure using CO_2/CH_4 (40/60) gas mixture.

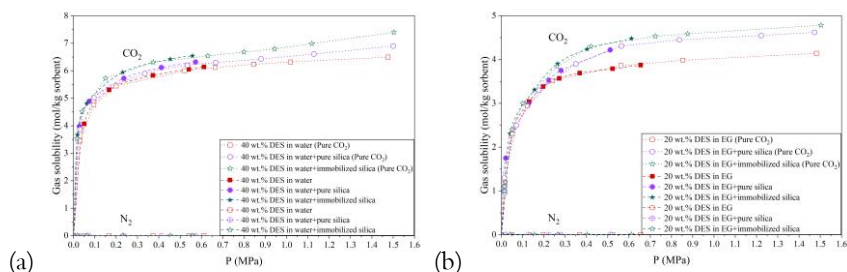


Fig. 3-18. Gas solubility of the developed (a) aqueous and (b) non-aqueous slurries at 30 °C as the function of pressure using CO_2/N_2 (25/75) gas mixture.

3.4.2 CO_2 sorption using conditioned flue gas from CHP boiler

The CO_2 capture performance of the developed aqueous and non-aqueous systems was evaluated using conditioned flue gas from CHP boiler (collected after pre-drying and particular removal through filtration) at atmospheric pressure and 25 °C. The obtained results are summarized in Figs. 3-19 (a) and (b).

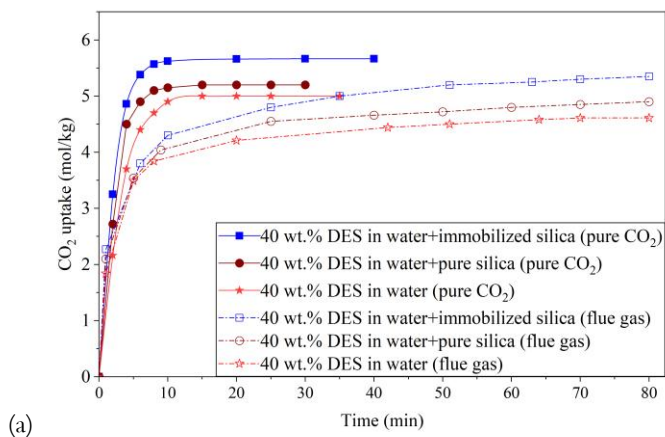
The CO_2 uptake (mol/kg) as a function of time using conditioned flue gas for the aqueous systems is presented in Fig. 3-19 (a), alongside previously reported data obtained under pure CO_2 for comparison [77, 81]. Under conditioned flue gas, all aqueous systems exhibit a moderately fast initial increase in CO_2 uptake, followed by a more gradual rise toward

equilibrium. The early-stage uptake is primarily governed by chemical interactions between CO_2 and the DES components, while the subsequent slower increase reflects diffusion limitations and reduced mass transfer rates. Compared to pure CO_2 , the initial slope is less steep and the time required to reach saturation is longer, which can be attributed to the lower partial pressure of CO_2 in the flue gas stream, resulting in a weaker driving force for sorption. Also, none of the aqueous systems reached saturation or exhibited a plateau in CO_2 uptake even after ~ 80 min. Instead, the uptake continued to increase, suggesting that longer time is required for these systems to achieve complete saturation when using conditioned flue gas. Among all, the aqueous slurry containing immobilized silica demonstrates the highest CO_2 uptake under conditioned flue gas. This enhanced performance can be attributed to improved mass transfer, as well as increased accessibility of reactive sites provided by the silica network. In contrast, systems without immobilized silica show relatively lower uptake and slower kinetics.

The CO_2 uptake behavior of the non-aqueous systems using the conditioned flue gas from CHP boiler is shown in Fig. 3-19 (b), together with corresponding data under pure CO_2 . Similar to the aqueous systems, a moderate initial increase in uptake is observed, followed by a gradual approach to equilibrium. However, the overall uptake is lower for non-aqueous systems. The reduced initial slope and extended equilibration time under conditioned flue gas again reflect the influence of lower CO_2 partial pressure, which limits the mass transfer driving force and slows down sorption kinetics. Similar to the aqueous systems, none of the samples reached saturation or exhibited a plateau in CO_2 uptake up to ~ 80 min and the uptake continued to increase, indicating that a longer time is required for these systems to achieve complete saturation when

exposed to conditioned flue gas. Within the non-aqueous systems, the slurry incorporating immobilized silica achieves the highest CO₂ uptake. The presence of silica enhances gas-liquid contact and facilitates more efficient transport of CO₂ to reactive sites, thereby improving performance relative to systems lacking solid support.

Overall, the lower CO₂ uptake of non-aqueous systems compared to aqueous ones can be attributed to their lower DES content and higher viscosity, both of which hinder mass transfer and reduce the accessibility of reactive sites. From a process perspective, these kinetic limitations can potentially be alleviated at larger scales through appropriate absorber design, such as increasing column height, optimizing packing materials, enhancing gas-liquid interfacial area, or extending residence time. Nevertheless, the higher viscosity of the system may impose additional challenges, including increased pressure drop and higher energy consumption during continuous operation.



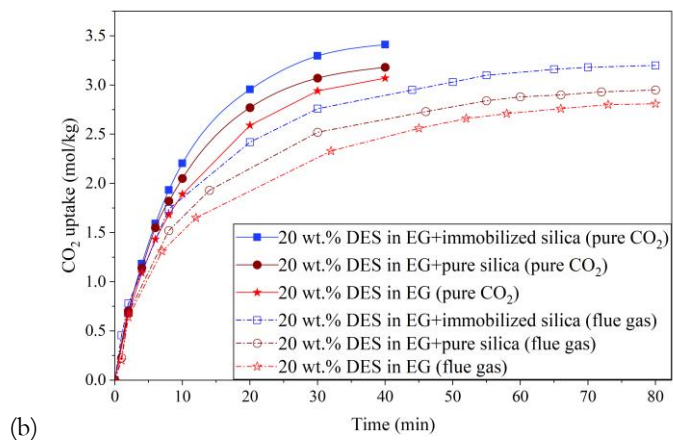


Fig. 3-19. CO₂ uptake of the developed (a) aqueous and (b) non-aqueous slurries 25 °C as the function of time using conditioned flue gas [77, 81].

Chapter 4

4 Conclusions

This work investigated the development and optimization of DES-based slurry systems for efficient CO₂ capture.

Aqueous DES development: [MEACl][EDA]-based DESs were successfully synthesized and evaluated as aqueous CO₂ absorbents. 40 wt.% aqueous [MEACl][EDA] (1:5) was identified as optimal, exhibiting higher CO₂ capture capacity and faster absorption kinetics than aqueous MEA, while maintaining comparable viscosity and good cyclic stability.

Integrated (immobilized + co-solvent added) DES systems: An integration strategy combining DES immobilization onto silica with co-solvent added DES was developed. The resulting slurries demonstrated improved CO₂ capture capacity, while preserving acceptable viscosity and long-term stability.

CO₂ desorption and regeneration behavior: The desorption characteristics of both aqueous and non-aqueous DES-based systems revealed efficient CO₂ release, high regeneration efficiencies, and strong thermal stability. In particular, non-aqueous slurries exhibited faster desorption kinetics, minimal solvent loss, and structural integrity.

Performance under conditioned flue gas: The CO₂ capture performance of the developed DES-based systems was evaluated using conditioned flue gas from CHP boiler. CO₂ uptake increased over time, albeit with slower sorption kinetics than under pure CO₂ conditions. This behavior is primarily attributed to the lower partial pressure of CO₂ in the conditioned flue gas stream. The presence of N₂, O₂, and trace amounts of CO and CH₄ had a negligible impact on the overall CO₂ uptake; however, the uptake profiles indicated that a longer time was

required to reach equilibrium compared to pure CO₂ conditions. Across all samples, slurries containing immobilized silica exhibited higher CO₂ uptake than those containing only pure solid or no solid content.

Moreover, the systems were further evaluated using synthetic CO₂/N₂ and CO₂/CH₄ mixtures over a wide pressure range. Increasing pressure enhanced CO₂ capture capacity for both aqueous and non-aqueous systems, with aqueous slurries consistently showing higher CO₂ capture capacities. Non-aqueous systems exhibited higher CH₄ uptake due to enhanced physical sorption in the EG phase.

Chapter 5

5 Future work

From a practical and scale-up perspective, further research is required on column and process design for slurry-based CO₂ capture systems. In particular, the hydrodynamic behavior of slurries must be carefully considered to prevent issues such as particle accumulation, settling, or plugging within process units, especially in conventional packed columns. Future studies should therefore focus on column configurations that are better suited for handling solid-liquid systems, such as slurry bubble columns, fluidized beds, or modified packing structures designed to minimize clogging while maintaining efficient gas-liquid contact. Additionally, optimizing flow dynamics, particle distribution, and mixing characteristics will be critical to ensure stable operation, enhanced mass transfer, and overall process efficiency in continuous systems. Further optimization of DES composition, immobilization strategies, and support materials could enable additional improvements in CO₂ selectivity, viscosity control, and mass transfer. In addition, comprehensive techno-economic and life-cycle assessments are recommended to quantify the energy demand, cost competitiveness, and environmental benefits of DES-based systems relative to established amine-based technologies, thereby facilitating their transition toward practical deployment.

Chapter 6

6 References

1. Xie, J., et al., *Financial expansion and CO₂ mitigation in top twenty emitters: Investigating the direct and moderating effects of the digital economy*. Gondwana Research, 2024. **125**: p. 1-14.
2. Martinez, M.M., *CO₂ capture from natural gas using ionic liquids: a thermodynamic study*. 2015.
3. Raimi, D., et al., *Global energy outlook 2024: Peaks or plateaus*. Resources for the Future: Washington, DC, USA, 2024.
4. Zhu, Y., et al., *Global Energy Outlook 2025: Headwinds and Tailwinds in the Energy Transition*. 2025, Resources for the Future.
5. Newell, R., et al., *Global energy outlook 2020: energy transition or energy addition*. Resources for the Future, 2020.
6. Rogelj, J., et al., *Mitigation pathways compatible with 1.5 C in the context of sustainable development*, in *Global warming of 1.5 C*. 2018, Intergovernmental Panel on Climate Change. p. 93-174.
7. Bashmakov, I.A., et al., *Climate Change 2022: Mitigation of Climate Change. Contribution of Working Group III to the Sixth Assessment Report of the Intergovernmental Panel on Climate Change, Chapter 11*. 2022.
8. Langie, K.M.G., et al., *Toward economical application of carbon capture and utilization technology with near-zero carbon emission*. Nature Communications, 2022. **13**(1): p. 7482.
9. Aresta, M., A. Dibenedetto, and A. Angelini, *The use of solar energy can enhance the conversion of carbon dioxide into energy-rich products: stepping towards artificial photosynthesis*. Philosophical Transactions of the Royal Society A: Mathematical, Physical and Engineering Sciences, 2013. **371**(1996): p. 20120111.
10. Nguyen-Trinh, H.A. and M. Ha-Duong, *Perspective of CO₂ capture & storage (CCS) development in Vietnam: Results from expert interviews*. International Journal of Greenhouse Gas Control, 2015. **37**: p. 220-227.

11. Nagireddi, S., J.R. Agarwal, and D. Vedapuri, *Carbon Dioxide Capture, Utilization, and Sequestration: Current Status, Challenges, and Future Prospects for Global Decarbonization*. ACS Engineering Au, 2023.
12. Cormos, A.-M., et al., *Carbon capture and utilisation technologies applied to energy conversion systems and other energy-intensive industrial applications*. Fuel, 2018. **211**: p. 883-890.
13. Fernandez, E.S., et al., *Thermodynamic assessment of amine based CO₂ capture technologies in power plants based on European Benchmarking Task Force methodology*. Fuel, 2014. **129**: p. 318-329.
14. Theo, W.L., et al., *Review of pre-combustion capture and ionic liquid in carbon capture and storage*. Applied energy, 2016. **183**: p. 1633-1663.
15. Pales, A.F. and S. Bennett, *Energy technology perspectives 2020*. 2020, Tech. Rep.). International Energy Agency. <https://www.iea.org/reports>
16. Gkotsis, P., E. Peleka, and A. Zouboulis, *Membrane-Based Technologies for Post-Combustion CO₂ Capture from Flue Gases: Recent Progress in Commonly Employed Membrane Materials*. Membranes, 2023. **13**(12): p. 898.
17. Song, C., et al., *Cryogenic-based CO₂ capture technologies: State-of-the-art developments and current challenges*. Renewable and sustainable energy reviews, 2019. **101**: p. 265-278.
18. Rochelle, G.T., *Amine scrubbing for CO₂ capture*. Science, 2009. **325**(5948): p. 1652-1654.
19. Khan, U., et al., *Assessing absorption-based CO₂ capture: Research progress and techno-economic assessment overview*. Carbon capture science & technology, 2023. **8**: p. 100125.
20. Ochedi, F.O., et al., *Carbon dioxide capture using liquid absorption methods: a review*. Environmental Chemistry Letters, 2021. **19**(1): p. 77-109.

21. Ochedi, F.O., et al., *Carbon dioxide capture using liquid absorption methods: a review*. Environmental Chemistry Letters, 2021. **19**: p. 77-109.
22. Spigarelli, B.P. and S.K. Kawatra, *Opportunities and challenges in carbon dioxide capture*. Journal of CO₂ Utilization, 2013. **1**: p. 69-87.
23. Zhang, C. *Absorption principle and techno-economic analysis of CO₂ absorption technologies: A review*. in *IOP Conference Series: Earth and Environmental Science*. 2021. IOP Publishing.
24. Isaacs, E.E., F.D. Otto, and A.E. Mather, *Solubility of mixtures of hydrogen sulfide and carbon dioxide in a monoethanolamine solution at low partial pressures*. Journal of Chemical and Engineering Data, 1980. **25**(2): p. 118-120.
25. Yu, C.-H., C.-H. Huang, and C.-S. Tan, *A review of CO₂ capture by absorption and adsorption*. Aerosol and Air Quality Research, 2012. **12**(5): p. 745-769.
26. Zhao, Z., et al., *Thermodynamic regulation of carbon dioxide capture by functionalized ionic liquids*. Chemical Society Reviews, 2025. **54**(4): p. 2091-2126.
27. Kwon, S., et al., *Innovative CO₂ capture via deep eutectic solvents: Molecular design, Mechanistic insights, and enhanced sorption in functionalized porous materials*. Chemical Engineering Journal, 2025. **503**: p. 158172.
28. Guo, L., et al., *A simplified semi-empirical model for modeling of CO₂ solubilities in aqueous MDEA and MEA solutions*. Fluid Phase Equilibria, 2022. **555**: p. 113352.
29. Shi, Q., *Development and Identification of Amine-based Deep Eutectic Solvents for CO₂ Capture*. 2025, Luleå University of Technology.
30. Vitillo, J.G., B. Smit, and L. Gagliardi, *Introduction: carbon capture and separation*. 2017, ACS Publications. p. 9521-9523.
31. White, C.M., et al., *Separation and capture of CO₂ from large stationary sources and sequestration in geological formations—coalbeds*

- and deep saline aquifers*. Journal of the Air & Waste Management Association, 2003. **53**(6): p. 645-715.
32. Nwaoha, C., et al., *Carbon dioxide (CO₂) capture: Absorption-desorption capabilities of 2-amino-2-methyl-1-propanol (AMP), piperazine (PZ) and monoethanolamine (MEA) tri-solvent blends*. Journal of Natural Gas Science and Engineering, 2016. **33**: p. 742-750.
 33. François, M.H.-J., et al., *CO₂ solubility and amine volatility data for low-concentration solutions of MEA, AMP, PZ and CESAR-1 blend (AMP/PZ)*. Results in Engineering, 2024. **22**: p. 102163.
 34. Brüder, P., et al. *CO₂ capture into aqueous solutions of the mixed solvent Cesar 1*. in *Proceedings of the 2nd Annual Gas Processing Symposium*. 2010. Elsevier.
 35. Wilkes, J.S., *A short history of ionic liquids—from molten salts to neoteric solvents*. Green Chemistry, 2002. **4**(2): p. 73-80.
 36. Figueroa, J.D., et al., *Advances in CO₂ capture technology—the US Department of Energy's Carbon Sequestration Program*. International journal of greenhouse gas control, 2008. **2**(1): p. 9-20.
 37. Singh, S.K. and A.W. Savoy, *Ionic liquids synthesis and applications: An overview*. Journal of Molecular Liquids, 2020. **297**: p. 112038.
 38. Xu, Y., et al., *Tuning ionic liquid-based functional deep eutectic solvents and other functional mixtures for CO₂ capture*. Chemical Engineering Journal, 2023. **463**: p. 142298.
 39. Foorginezhad, S., *CO₂ Capture through Integration of Aqueous and Immobilized Deep Eutectic Solvents*. 2024, Luleå University of Technology.
 40. Anthony, J.L., et al., *Anion effects on gas solubility in ionic liquids*. The Journal of Physical Chemistry B, 2005. **109**(13): p. 6366-6374.
 41. Bates, E.D., et al., *CO₂ capture by a task-specific ionic liquid*. Journal of the American Chemical Society, 2002. **124**(6): p. 926-927.

42. Abbott, A.P., et al., *Deep eutectic solvents formed between choline chloride and carboxylic acids: versatile alternatives to ionic liquids*. Journal of the American Chemical Society, 2004. **126**(29): p. 9142-9147.
43. Abbott, A.P., et al., *Preparation of novel, moisture-stable, Lewis-acidic ionic liquids containing quaternary ammonium salts with functional side chains* Electronic supplementary information (ESI) available: plot of conductivity vs. temperature for the ionic liquid formed from zinc chloride and choline chloride (2: 1). See <http://www.rsc.org/suppdata/cc/b1/b106357j>. Chemical communications, 2001(19): p. 2010-2011.
44. Tomé, L.I., et al., *Deep eutectic solvents for the production and application of new materials*. Applied Materials Today, 2018. **10**: p. 30-50.
45. Mu, L., et al., *Research progress on deep eutectic solvents and recent applications*. Processes, 2023. **11**(7): p. 1986.
46. Sarmad, S., J.P. Mikkola, and X. Ji, *Carbon dioxide capture with ionic liquids and deep eutectic solvents: a new generation of sorbents*. ChemSusChem, 2017. **10**(2): p. 324-352.
47. Quintana, A.A., et al., *Enabling sustainable chemistry with ionic liquids and deep eutectic solvents: a fad or the future?* Angewandte Chemie International Edition, 2022. **61**(37): p. e202205609.
48. Li, X., et al., *Solubility of CO₂ in a choline chloride+ urea eutectic mixture*. Journal of Chemical & Engineering Data, 2008. **53**(2): p. 548-550.
49. Sarmad, S., et al., *Screening of deep eutectic solvents (DESs) as green CO₂ sorbents: from solubility to viscosity*. New Journal of Chemistry, 2017. **41**(1): p. 290-301.
50. Foorginezhad, S., G. Yu, and X. Ji, *Reviewing and screening ionic liquids and deep eutectic solvents for effective CO₂ capture*. Frontiers in Chemistry, 2022. **10**: p. 951951.
51. Foorginezhad, S. and X. Ji, *Development of monoethanolamine chloride-ethylene diamine deep eutectic solvent for efficient carbon dioxide*

- capture*. Separation and Purification Technology, 2024. **347**: p. 127593.
52. Cichowska-Kopczyńska, I., B. Nowosielski, and D. Warmińska, *Deep eutectic solvents: properties and applications in CO₂ separation*. Molecules, 2023. **28**(14): p. 5293.
 53. Kumar, K. and A. Kumar, *Enhanced CO₂ adsorption and separation in ionic-liquid-impregnated mesoporous silica MCM-41: a molecular simulation study*. The Journal of Physical Chemistry C, 2018. **122**(15): p. 8216-8227.
 54. Polesso, B.B., et al., *Imidazolium-based ionic liquids impregnated in silica and alumina supports for CO₂ capture*. Materials Research, 2019. **22**: p. e20180810.
 55. Luo, Q. and E. Pentzer, *Encapsulation of ionic liquids for tailored applications*. ACS applied materials & interfaces, 2019. **12**(5): p. 5169-5176.
 56. Gao, S., et al., *Ionic liquid functionalized 3D mesoporous FDU-12 for effective SO₂ capture*. ACS Sustainable Chemistry & Engineering, 2019. **8**(1): p. 586-593.
 57. Uehara, Y., D. Karami, and N. Mahinpey, *CO₂ adsorption using amino acid ionic liquid-impregnated mesoporous silica sorbents with different textural properties*. Microporous and Mesoporous Materials, 2019. **278**: p. 378-386.
 58. Xue, C., et al., *Pyridine-containing ionic liquids lowly loaded in large mesoporous silica and their rapid CO₂ gas adsorption at low partial pressure*. Journal of CO₂ Utilization, 2019. **34**: p. 282-292.
 59. Foorginezhad, S. and X. Ji, *Immobilized ionic liquids/deep eutectic solvents in carbon capture: current progress and future potential*. Clean Technologies and Environmental Policy, 2025: p. 1-17.
 60. Foorginezhad, S., et al., *Review and analysis of porous adsorbents for effective CO₂ capture*. Renewable and Sustainable Energy Reviews, 2025. **215**: p. 115589.

61. Xie, W., et al., *Mass transfer rate enhancement for CO₂ separation by ionic liquids: effect of film thickness*. Industrial & Engineering Chemistry Research, 2016. **55**(1): p. 366-372.
62. Lee, J.W., et al., *Review of nanoabsorbents for capture enhancement of CO₂ and its industrial applications with design criteria*. Renewable and Sustainable Energy Reviews, 2021. **138**: p. 110524.
63. Yu, W., et al., *Review of liquid nano-absorbents for enhanced CO₂ capture*. Nanoscale, 2019. **11**(37): p. 17137-17156.
64. Salih, H.A., et al., *Hybrid-Slurry/Nanofluid systems as alternative to conventional chemical absorption for carbon dioxide capture: A review*. International Journal of Greenhouse Gas Control, 2021. **110**: p. 103415.
65. Wang, T., et al., *Enhanced CO₂ absorption and desorption by monoethanolamine (MEA)-based nanoparticle suspensions*. Industrial & Engineering Chemistry Research, 2016. **55**(28): p. 7830-7838.
66. Suresh, S., et al., *Synthesis of Al₂O₃-Cu/water hybrid nanofluids using two step method and its thermo physical properties*. Colloids and Surfaces A: Physicochemical and Engineering Aspects, 2011. **388**(1-3): p. 41-48.
67. Jiang, J., et al., *Experimental study of CO₂ absorption in aqueous MEA and MDEA solutions enhanced by nanoparticles*. International Journal of greenhouse gas control, 2014. **29**: p. 135-141.
68. Karve, S. and V. Juvekar, *Gas absorption into slurries containing fine catalyst particles*. Chemical engineering science, 1990. **45**(3): p. 587-594.
69. Li, H., et al., *CO₂ capture using ZIF-8/water-glycol-2-methylimidazole slurry with high capacity and low desorption heat*. Chemical Engineering Science, 2018. **182**: p. 189-199.
70. Yang, M.-K., et al., *Separation of IGCC syngas by using ZIF-8/dimethylacetamide slurry with high CO₂ sorption capacity and sorption speed but low sorption heat*. Energy, 2020. **201**: p. 117605.

71. Park, S.W., B.S. Choi, and J.W. Lee, *Chemical absorption of carbon dioxide into aqueous colloidal silica solution with diethanolamine*. Separation science and technology, 2006. **41**(14): p. 3265–3278.
72. Liu, F., et al., *Novel amino-functionalized ionic liquid/organic solvent with low viscosity for CO₂ capture*. Environmental Science & Technology, 2020. **54**(6): p. 3520–3529.
73. Gao, G., et al., *Novel assessment of highly efficient polyamines for post-combustion CO₂ capture: Absorption heat, reaction rate, CO₂ cyclic capacity, and phase change behavior*. Separation and Purification Technology, 2023. **306**: p. 122615.
74. Wang, R., et al., *Development of biphasic solvent for CO₂ capture by tailoring the polarity of amine solution*. Fuel, 2022. **325**: p. 124885.
75. Meng, F., et al., *Study on absorption and regeneration performance of EHA-DMSO non-aqueous absorbent for CO₂ capture from flue gas*. Energy, 2024. **286**: p. 129631.
76. Trivedi, T.J., et al., *Deep eutectic solvents as attractive media for CO₂ capture*. Green Chemistry, 2016. **18**(9): p. 2834–2842.
77. Foorginezhad, S. and X. Ji, *Developing non-aqueous slurry for CO₂ capture*. Carbon Capture Science & Technology, 2025. **15**: p. 100385.
78. Zhang, Z., et al., *Preparation and SO₂ sorption/desorption behavior of an ionic liquid supported on porous silica particles*. Industrial & engineering chemistry research, 2009. **48**(4): p. 2142–2148.
79. Uehara, Y., D. Karami, and N. Mahinpey, *Amino acid ionic liquid-modified mesoporous silica sorbents with remaining surfactant for CO₂ capture*. Adsorption, 2019. **25**: p. 703–716.
80. Wang, X., et al., *Enhanced CO₂ capture by binary systems of pyridinium-based ionic liquids and porous ZIF-8 particles*. The Journal of Chemical Thermodynamics, 2019. **128**: p. 415–423.
81. Foorginezhad, S. and X. Ji, *Developing slurry based on immobilized and aqueous [MEACl][EDA] for CO₂ capture*. Chemical Engineering Journal, 2024. **499**: p. 156176.

82. Tsionopoulos, C., *An empirical correlation of second virial coefficients*. AIChE Journal, 1974. **20**(2): p. 263-272.
83. Prausnitz, J.M., R.N. Lichtenthaler, and E.G. De Azevedo, *Molecular thermodynamics of fluid-phase equilibria*. 1998: Pearson Education.
84. Adkins, C.J., *Equilibrium thermodynamics*. 1983: Cambridge University Press.
85. Yu, H., et al., *Low viscosity amino acid ionic liquids with asymmetric tetraalkylammonium cations for fast absorption of CO₂*. New Journal of Chemistry, 2009. **33**(12): p. 2385-2390.
86. Li, Z., et al., *Study of CO₂ absorption/desorption behaviors in aqueous (2-hydroxyethyl)-trimethyl-ammonium (S)-2-pyrrolidine-carboxylic acid salt ([Cho][Pro])⁺ K₂CO₃ solutions*. International Journal of Greenhouse Gas Control, 2019. **83**: p. 51-60.
87. Liu, Y., et al., *Studies of CO₂ absorption/regeneration performances of novel aqueous monoethanolamine (MEA)-based solutions*. Journal of Cleaner Production, 2016. **112**: p. 4012-4021.
88. Abranches, D.O. and J.A. Coutinho, *Everything you wanted to know about deep eutectic solvents but were afraid to be told*. Annual Review of Chemical and Biomolecular Engineering, 2023. **14**: p. 141-163.
89. Lee, M.-J., et al., *Solid–Liquid Equilibria for 4-Methoxyphenol with Catechol, Ethylenediamine, or Piperazine*. Journal of Chemical & Engineering Data, 1997. **42**(2): p. 349-352.
90. Foorginezhad, S. and X. Ji, *Development of monoethanolamine chloride-Ethylene diamine deep eutectic solvent for efficient carbon dioxide capture*. Separation and Purification Technology, 2024: p. 127593.
91. Agcieienko, V. and R. Buchner, *Is ethaline a deep eutectic solvent?* Physical Chemistry Chemical Physics, 2022. **24**(9): p. 5265-5268.

92. Kollau, L.J., et al., *Quantification of the liquid window of deep eutectic solvents*. Chemical communications, 2018. **54**(95): p. 13351-13354.
93. Martins, M.A., S.P. Pinho, and J.A. Coutinho, *Insights into the nature of eutectic and deep eutectic mixtures*. Journal of Solution Chemistry, 2019. **48**: p. 962-982.
94. Milevskii, N., et al., *Separation of Li (I), Co (II), Ni (II), Mn (II), and Fe (III) from hydrochloric acid solution using a menthol-based hydrophobic deep eutectic solvent*. Hydrometallurgy, 2022. **207**: p. 105777.
95. El Achkar, T., H. Greige-Gerges, and S. Fourmentin, *Basics and properties of deep eutectic solvents: a review*. Environmental chemistry letters, 2021. **19**: p. 3397-3408.
96. Shishov, A., et al., *Deep eutectic solvents or eutectic mixtures? Characterization of tetrabutylammonium bromide and nonanoic acid mixtures*. The Journal of Physical Chemistry B, 2022. **126**(21): p. 3889-3896.
97. Yan, X., et al., *Amine-modified SBA-15: effect of pore structure on the performance for CO₂ capture*. Industrial & Engineering Chemistry Research, 2011. **50**(6): p. 3220-3226.
98. Hiyoshi, N., K. Yogo, and T. Yashima, *Adsorption characteristics of carbon dioxide on organically functionalized SBA-15*. Microporous and Mesoporous Materials, 2005. **84**(1-3): p. 357-365.
99. Shukla, S.K., et al., *Superior gravimetric CO₂ uptake of aqueous deep-eutectic solvent solutions*. Chemical Communications, 2023. **59**(70): p. 10516-10519.
100. Liu, X., et al., *CO₂ capture by alcohol ammonia based deep eutectic solvents with different water content*. Materials Research Express, 2022. **9**(1): p. 015504.
101. Bi, Y., et al., *Efficient CO₂ capture by a novel deep eutectic solvent through facile, one-pot synthesis with low energy consumption and feasible regeneration*. Science of The Total Environment, 2020. **705**: p. 135798.

102. Pasha, M., et al., *CO₂ absorption with diamine functionalized deep eutectic solvents in microstructured reactors*. *Process Safety and Environmental Protection*, 2022. **159**: p. 106-119.
103. Zhang, Y., et al., *CO₂ absorption performance of ChCl-MEA deep eutectic solvent in microchannel*. *Journal of Environmental Chemical Engineering*, 2022. **10**(6): p. 108792.
104. Mjalli, F.S., et al., *Monoethanolamine-based deep eutectic solvents, their synthesis and characterization*. *Fluid Phase Equilibria*, 2017. **448**: p. 30-40.
105. Dong, W., et al., *The preparation of ethylenediamine - modified fluorescent carbon dots and their use in imaging of cells*. *Luminescence*, 2015. **30**(6): p. 867-871.
106. Gabriele, F., et al., *Effect of water addition on choline chloride/glycol deep eutectic solvents: Characterization of their structural and physicochemical properties*. *Journal of Molecular Liquids*, 2019. **291**: p. 111301.
107. Wibowo, H., et al., *Experimental study on the effect of water addition to ChCl-MEA DES towards its performance in CO₂ removal from syngas*. *Biomass Conversion and Biorefinery*, 2022: p. 1-11.
108. Wang, C., et al., *Equimolar CO₂ capture by imidazolium-based ionic liquids and superbase systems*. *Green chemistry*, 2010. **12**(11): p. 2019-2023.
109. Mergler, Y., et al., *Solvents for CO₂ capture. Structure-activity relationships combined with vapour-liquid-equilibrium measurements*. *Energy Procedia*, 2011. **4**: p. 259-266.
110. Jackson, P., et al., *In situ Fourier Transform-Infrared (FT-IR) analysis of carbon dioxide absorption and desorption in amine solutions*. *Energy Procedia*, 2009. **1**(1): p. 985-994.
111. Li, F., et al., *Protic ionic liquids with low viscosity for efficient and reversible capture of carbon dioxide*. *International Journal of Greenhouse Gas Control*, 2019. **90**: p. 102801.
112. Yan, M., et al., *Effect of operating parameters on CO₂ capture from biogas with choline chloride—monoethanolamine deep eutectic solvent*

- and its aqueous solution*. Biomass Conversion and Biorefinery, 2024. **14**(1): p. 283-297.
113. Shi, S., S. Li, and X. Liu, *Mechanism Study of Imidazole-Type Deep Eutectic Solvents for Efficient Absorption of CO₂*. ACS omega, 2022. **7**(51): p. 48272-48281.
 114. Huan, Q., et al., *Study on regeneration characteristics of choline chloride-monoethanolamine deep eutectic solvent after capturing CO₂ from biogas*. Separation and Purification Technology, 2022. **302**: p. 122064.
 115. Mohamedali, M., H. Ibrahim, and A. Henni, *Imidazolium based ionic liquids confined into mesoporous silica MCM-41 and SBA-15 for carbon dioxide capture*. Microporous and Mesoporous Materials, 2020. **294**: p. 109916.
 116. Taheri, M., et al., *Simultaneous absorption of carbon dioxide (CO₂) and hydrogen sulfide (H₂S) from CO₂-H₂S-CH₄ gas mixture using amine-based nanofluids in a wetted wall column*. Journal of natural gas science and engineering, 2016. **28**: p. 410-417.
 117. Lee, J.W., et al., *CO₂ bubble absorption enhancement in methanol-based nanofluids*. International journal of refrigeration, 2011. **34**(8): p. 1727-1733.
 118. Gao, S., et al., *Potassium carbonate slurry-based CO₂ capture technology*. Energy & fuels, 2015. **29**(10): p. 6656-6663.
 119. Marliza, T., et al., *CO₂ capture using ionic liquid hybrid sorbent: physical and chemical adsorption-desorption study*. Materials Today: Proceedings, 2022. **64**: p. 20-26.
 120. Wu, N., et al., *Confinement phenomenon effect on the CO₂ absorption working capacity in ionic liquids immobilized into porous solid supports*. Langmuir, 2017. **33**(42): p. 11719-11726.
 121. Wang, X., et al., *Amino acid-functionalized ionic liquid solid sorbents for post-combustion carbon capture*. ACS applied materials & interfaces, 2013. **5**(17): p. 8670-8677.

122. Choi, S.-w. and H.-K. Bae, *Adsorption of CO₂ on amine-impregnated mesoporous MCM41 silica*. KSCE Journal of Civil Engineering, 2014. **18**: p. 1977-1983.
123. Huang, H.Y., et al., *Amine-grafted MCM-48 and silica xerogel as superior sorbents for acidic gas removal from natural gas*. Industrial & Engineering Chemistry Research, 2003. **42**(12): p. 2427-2433.
124. Wang, X., et al., *Infrared study of CO₂ sorption over "molecular basket" sorbent consisting of polyethylenimine-modified mesoporous molecular sieve*. The Journal of Physical Chemistry C, 2009. **113**(17): p. 7260-7268.
125. Chiang, C.-H., H. Ishida, and J.L. Koenig, *The structure of γ -aminopropyltriethoxysilane on glass surfaces*. Journal of Colloid and Interface Science, 1980. **74**(2): p. 396-404.
126. Culler, S., H. Ishida, and J. Koenig, *Structure of silane coupling agents adsorbed on silicon powder*. Journal of colloid and interface science, 1985. **106**(2): p. 334-346.
127. Rovani, S., et al., *An alternative and simple method for the preparation of bare silica nanoparticles using sugarcane waste ash, an abundant and despised residue in the Brazilian industry*. Journal of the Brazilian Chemical Society, 2019. **30**: p. 1524-1533.
128. Loganathan, S., M. Tikmani, and A.K. Ghoshal, *Novel pore-expanded MCM-41 for CO₂ capture: synthesis and characterization*. Langmuir, 2013. **29**(10): p. 3491-3499.
129. Cui, S., et al., *Mesoporous amine-modified SiO₂ aerogel: a potential CO₂ sorbent*. Energy & environmental science, 2011. **4**(6): p. 2070-2074.
130. Saravanan, S. and R. Dubey, *Synthesis of SiO₂ nanoparticles by sol-gel method and their optical and structural properties*. Rom. J. Inf. Sci. Technol, 2020. **23**(1): p. 105-112.
131. Richner, G. and G. Puxty, *Assessing the chemical speciation during CO₂ absorption by aqueous amines using in situ FTIR*. Industrial & Engineering Chemistry Research, 2012. **51**(44): p. 14317-14324.

Department of Engineering Sciences and Mathematics
Division of Energy Science

ISSN 1402-1544
ISBN 978-91-8048-997-3 (print)
ISBN 978-91-8048-998-0 (pdf)

Luleå University of Technology 2026

